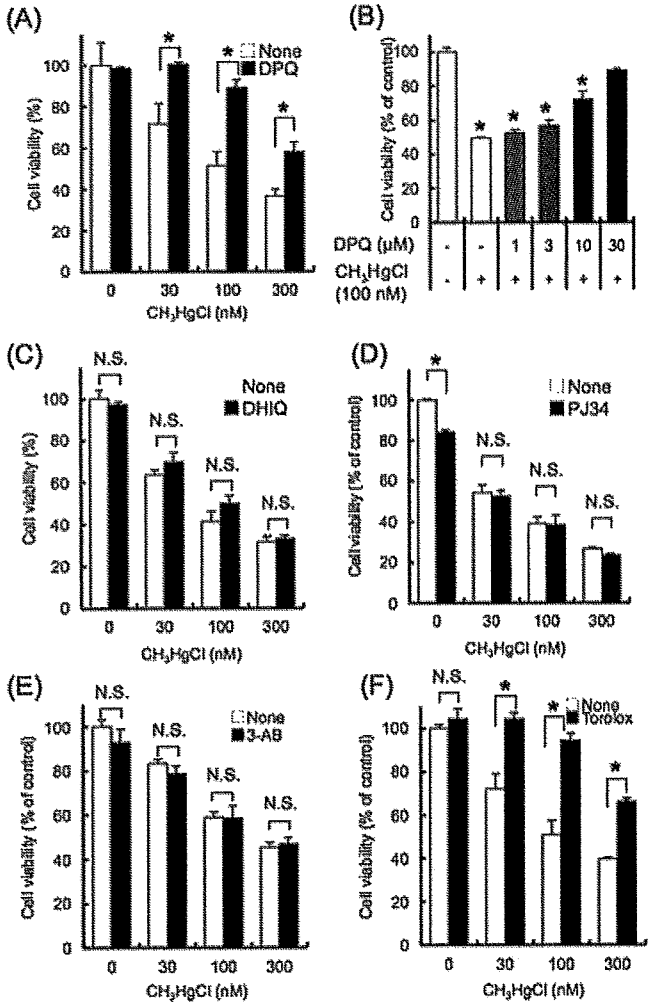

Fig. 1. Effects of PARP inhibitors on methylmercury-induced cytotoxicity in primary culture of rat CGCs. CGC viability was assayed 48 hr after treatment of methylmercury. Reagents, DPQ at 30 μM (**A,B**), DHIQ at 30 μM (**C**), PJ34 at 10 μM (**D**), 3-AB at 1 mM (**E**), and Torolox at 50 μM (**F**), were treated 30 min before methylmercury treatment and then were coincubated with methylmercury for 48 hr. Data are expressed as the percentage of cell viability compared with the control group, mean ± SD ($n = 3$). Asterisks indicate data that are significantly different ($P < 0.05$). n.s. in figures indicates that there is no statistically significant difference between the data.

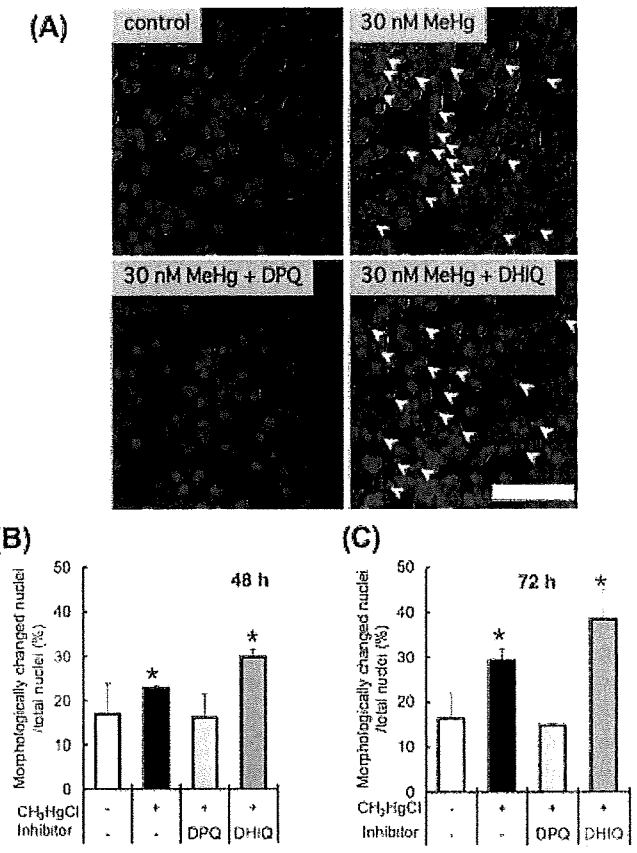

Fig. 2. Protective effects of DPQ on the methylmercury-induced morphological changes of nuclei in CGCs. Primary cultures of rat CGC were exposed at 30 nM methylmercury 30 min after PARP inhibitor treatments with DPQ and DHIQ. (**A**) Microphotographs of the cells stained by Hoechst 33258 48 hr after methylmercury treatment. Arrowheads indicate the condensed and fragmented nuclei. Scale bar = 50 μm. (B,C) Ratio of morphologically changed nuclear number to total nuclear number. These conditions of treatment were determined in preliminary experiments. Results are shown (**B**) 48 hr and (**C**) 72 hr after treatment with methylmercury. Data are expressed as percentage of abnormal nuclei compared with the total number of nuclei, mean ± SD ($n = 3$). Asterisks indicate data that are significantly different compared with control ($P < 0.01$).

morphologically abnormal nuclei. These results indicate that the protective effect of DPQ against methylmercury-induced cell death involves mechanisms other than PARP inhibition.

Effect of DPQ on GSH Depletion-induced Cell Death and Intracellular Total GSH Level

A decrease of GSH is observed in methylmercury-treated cells and accelerates the methylmercury-induced cell death of CGCs (Kaur et al., 2006). GSH, the major intracellular antioxidant, reduces ROS and methylmercury cytotoxicity in vitro. Then we investigated the effect of DPQ on a cell death model of CGCs and IMR-32 cells via treatment of GSH reducers, BSO or DEM. BSO at 300 μM for 72 hr or DEM at 200 μM for 24 hr treatment caused a decrease of cell viability in the primary culture of CGCs to 54.0% and 54.7%, respectively (Fig. 3A,B). The viabilities of IMR-32 cells treated with BSO at 300 μM for 48 hr or DEM at 50 μM for 24 hr were also decreased compared with that of control cells to 11.8% or 43.7% (Fig. 3C,D), respectively. DPQ cotreatment significantly affected the decrease of cell viability levels caused by BSO/DEM treatment, which were restored to approximately 80% and 90% in CGCs and IMR-32 cells (Fig. 3A–D), respectively. On the other hand, neither DHIQ nor 3-AB affected BSO- or DEM-induced cytotoxicity in CGCs and IMR-32 cells. Because DPQ had a protective effect against GSH reducers, we hypothesized that DPQ

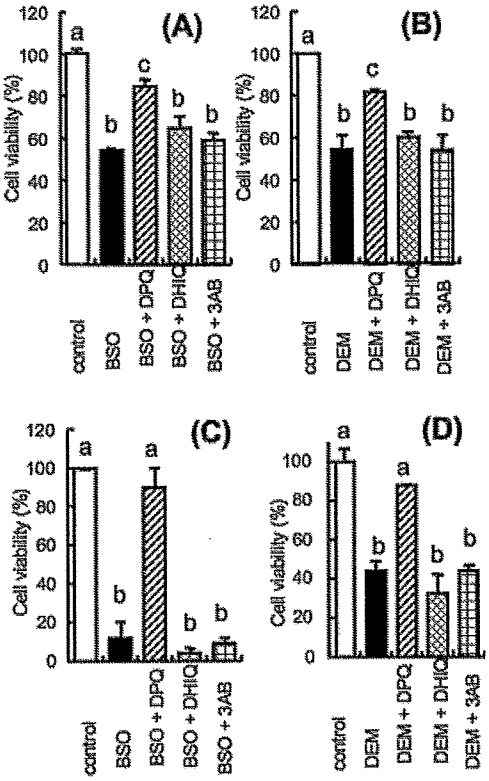

Fig. 3. Effects of PARP inhibitors on GSH depletion-induced cytotoxicity in vitro. Primary cultures of rat CGCs (**A,B**) and human neuroblastoma IMR-32 cells (**C,D**) were incubated in medium containing PARP inhibitors and GSH reducers buthionine-sulfoximine (BSO) (A,C), DEM (B,D). The treatment of BSO or DEM is (A) at 300 μM for 72 hr, (B) at 200 μM for 24 hr, (C) at 300 μM for 48 hr and (D) at 50 μM for 24 hr. These conditions of treatment were determined in preliminary experiments. The cells were pretreated with PARP inhibitors, DPQ (30 μM), DHIQ (30 μM) and 3-AB (1 mM), 1 hr before BSO or DEM treatment. The concentrations of PARP inhibitors were the highest concentration at which the PARP inhibitors had no affect effect on cell viability. Data are expressed as the percentage of cell viability compared with the control group, mean ± SD ($n = 3$). Bars with different lowercase letters are significantly different ($P < 0.05$) from one another.

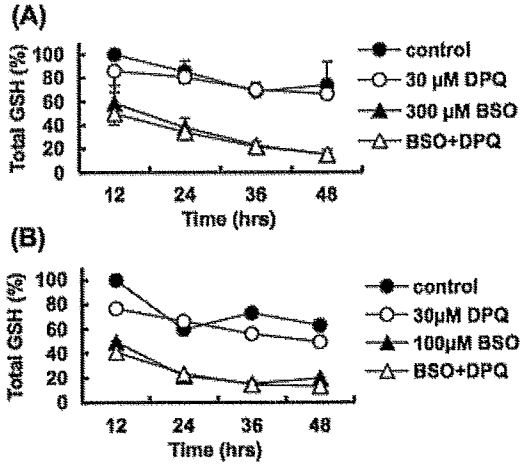

Fig. 4. Cellular total GSH levels in the BSO- and DPQ-treated cells, (**A**) rat CGCs, and (**B**) human neuroblastoma IMR-32 cells. The cells were treated with DPQ or BSO for the times indicated. Data are indicated as percentage compared with control group at 12 hr, mean ± SD ($n = 3$).

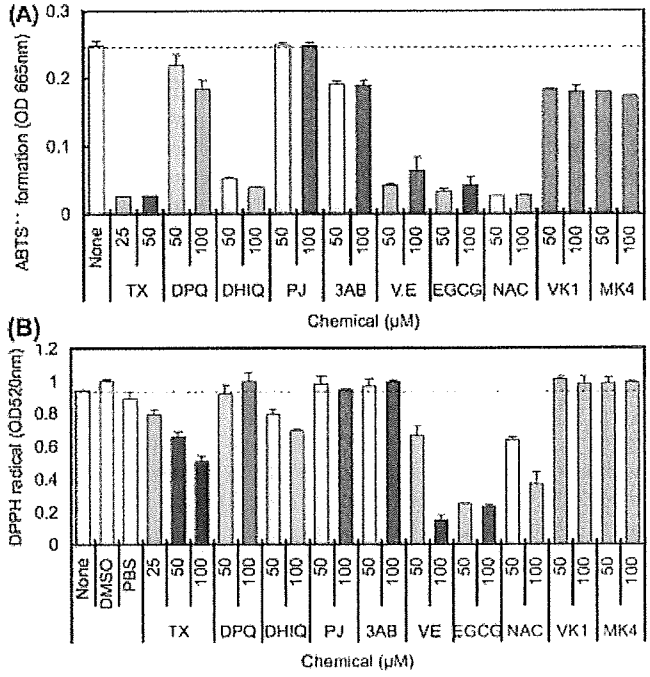

Fig. 5. Radical scavenging activities of PARP inhibitors. (**A**) Antioxidant activity assay by using ABTS cation ($ABTS^{+\bullet}$) formation with H_2O_2 as the oxidant trigger. $ABTS^{+\bullet}$ was measured by optical absorbance at 665 nm. (**B**) Free radicals, which have absorption at 520 nm, are generated by DPPH in solution. The scavenging of the radicals was assayed spectrophotometrically after the addition of DPQ, other PARP inhibitors or antioxidants at 520 nm. Data are expressed as mean ± SD ($n = 3$).

has the ability to increase cellular GSH level, then tested the hypothesis by measuring total GSH in BSO-treated cells and controls, and those cotreated with DPQ. BSO treatment significantly decreased the GSH level compared with the control level at each incubation time in CGCs and IMR-32 cells (Fig. 4). Unexpectedly, DPQ did not significantly bring the BSO-induced decrement of GSH level back to the control level in CGCs and IMR-32, although DPQ did show a protective effect against cell death caused by GSH depletion, as shown in Figure 3A,C.

Direct Antioxidant Activity of DPQ Against Radicals

Involvement of ROS in the toxicity of methylmercury has been established (Ganther, 1978; Sarafian and Verity, 1991). Moreover, antioxidants inhibit the cytotoxicity of methylmercury in primary neuronal cultures (Park et al., 1996; Gassó et al., 2001). If DPQ directly scavenges ROS, that would account for the protective

effect of DPQ on the methylmercury cytotoxicity in the primary culture.

To determine the potential of DPQ as a direct scavenger against radicals, we used two antioxidant methods, the $ABTS^{+\bullet}$ formation method and the DPPH radical method. These methods use $ABTS^{+\bullet}$ or DPPH as radicals, respectively. Widely used antioxidants, e.g., vitamin E, NAC, EGCG, and Trolox, significantly diminished the radicals in both of these methods. Among PARP inhibitors such as DPQ, DHIQ, PJ34, and 3-AB, DHIQ clearly had the strongest scavenging potential against the radicals. Its potential was approximately five times (Fig. 5, top) and 1.3 times (Fig. 5, bottom) greater than that of DPQ in the $ABTS^{+\bullet}$ formation method and the DPPH radical method, respectively. The other compounds, PJ34, 3-AB, VK_1, and MK4, had almost the same radical scavenging activity as DPQ in both methods. In those assay, vitamin K was used as a negative control that has no ability to scavenge these radicals (Li et al., 2003).

DISCUSSION

Methylmercury at lower concentrations, ≤ 1 μM, induces cell death (apoptosis) in rat CGC culture, independent of the caspase cascade (Castoldi et al., 2000; Dare et al., 2000, 2001). PARP is activated via DNA damage and catalyzes the covalent attachment of ADP-ribose units from NAD^+ to chromatin-interacting proteins, such as histones, p53, DNA topoisomerase, and PARP-1 itself, which regulates nuclear homeostasis and assists in DNA repair (D'Amours et al., 1999). Additional stronger genotoxic stress than that in physiological state, however, causes the overactivation of PARP, resulting in hyper poly(ADP-ribosyl)ation- and PARP-dependent cell death. Thus, we hypothesized that the methylmercury-induced cell death of rat primary cultured CGCs at low concentrations is caused by PARP activation because a previous study showed that PARP is activated in when human lymphocytes die as a result of methylmercury treatment (Guo et al., 1998). In the present study, the involvement of PARP activation in cell death induced by methylmercury treatment was investigated by means of PARP inhibitors in primary cultured CGCs. If the cell death mechanism involved PARP activation, not only would DPQ treatment prevent cell death, but treatments by other PARP inhibitors (DHIQ, PJ34, and 3-AB) would as well. We found that among the PARP inhibitors, only DPQ inhibited cell death (Figs. 1 and 2). Additionally, Western blot test detected no poly(ADP-ribose) modification of PARP itself or of any other proteins in extracts of methylmercury-treated cells in the primary culture (data not shown). These results indicate that the methylmercury-induced cell death of CGCs does not involve PARP activation.

GSH is the most predominant intracellular thiol and acts as a major cellular antioxidant (Meister and Andersson, 1983). GSH modulators affect the methylmercury-treated cell viability in primary cultured neurons; NAC, a GSH precursor, increases the viability, and DEM, a reducer of GSH level, decreases it. In other words, the total amount of GSH is decreased in methylmercury-treated neural cells, primary cultured neurons, PC12 cells and GT1-7 cells (Sarafian et al., 1994; Kaur et al., 2006), and NAC treatment supplies the decrement of ROS to rescue primary cultured neurons from methylmercury-induced cell death (Park et al., 1996; Kaur et al., 2006). Therefore, in this study, we investigated the effect of DPQ on cell death of CGCs and IMR-32 cells through treatments of BSO and DEM. DPQ showed a protective effect against the cytotoxicity via treatment of GSH reducers in CGCs and IMR-32 cells. Furthermore, in DPQ's protection of CGCs, the BSO-induced reduction of cellular GSH was not restored (Figs. 3 and 4). These results exclude the influence of intracellular GSH levels from the protective effect of DPQ on GSH-depletion-induced cell death.

The involvement of oxidative stress in the process of methylmercury cytotoxicity has been hypothesized (Ganther, 1978; Sarafian and Verity, 1991). We found that Trolox, a widely used antioxidant, prevented methylmercury-induced cell death in CGC culture in this study (Fig. 1F), and results of previous reports showed that other antioxidants inhibited cell death in methylmercury-treated neuron cultures (Park et al., 1996; Gassó et al., 2001). To elucidate whether DPQ itself has the ability to scavenge radicals, we detected the antioxidant activity of DPQ by using $ABTS^{+\bullet}$ formation and DPPH radical methods. The potential of DPQ as a direct radical scavenger was considerably less than that of the other PARP inhibitors, while DHIQ had the strongest potential to scavenge radicals among the tested PARP inhibitors (Fig. 5). These results are congruent with those reported by Czapski et al. (2004) that DPQ has no effect on free radical reactions, i.e., protein oxidation or lipid peroxidation, while DHIQ and 3-AB possess antioxidative properties. In light of accruing evidence, a plausible explanation is that antioxidant activity of DPQ is not directly involved in its protective effect against methylmercury-induced cell death. Therefore, the data from the present study indicate that DPQ should be an efficient substance to protect cells from methylmercury and GSH-depletion neurotoxicity, and the results further suggest that DPQ's activity as a PARP inhibitor is not involved in the protection mechanisms of DPQ treatment. DPQ may reduce neuronal degradation via some activity other than inhibiting PARP and scavenging ROS. Thus, activities of DPQ other than PARP inhibition should be considered when evaluating the protective effect of DPQ, although there are some reports that DPQ as a PARP inhibitor prevents PARP activation and rescues the cells from neuronal degradation conditions (Eliasson et al., 1997; Takahashi et al., 1999; Meli et al., 2003; Ying et al., 2005).

It was noteworthy that coincubation with DPQ for more than 24 hr before cells normally start to die was needed for DPQ to exert a protective effect against the

methylmercury-induced cell death (data not shown). DPQ treatment may bring about some gene expression of antioxidative or neuroprotective genes that contribute to the protection against cell death through methylmercury, BSO or DEM treatment—e.g., bcl-2, manganese–superoxide dismutase, and metallothionein from increases of the relevant gene expressions prevent methylmercury-induced cell death (Kane et al., 1993; Aschner, 1997; Naganuma et al., 1998). Clarifying the target factor and the mechanism of the protective effect of DPQ against methylmercury-induced cell death will provide novel information about the mechanism of methylmercury cytotoxicity.

REFERENCES

Aito H, Aalto KT, Raivio KO. 2004. Adenine nucleotide metabolism and cell fate after oxidant exposure of rat cortical neurons: effects of inhibition of poly(ADP-ribose) polymerase. Brain Res 1013:117–124.

Aschner M. 1997. Astrocyte metallothioneins (MTs) and their neuroprotective role. Ann N Y Acad Sci 825:334–347.

Banasik M, Komura H, Shimoyama M, Ueda K. 1992. Specific inhibitors of poly(ADP-ribose) synthetase and mono(ADP-ribosyl) transferase. J Biol Chem 267:1569–1575.

Besson VC, Zsengeller Z, Plotkine M, Szabo C, Marchand-Verrecchia C. 2005. Beneficial effects of PJ34 and INO-1001, two novel water-soluble poly(ADP-ribose) polymerase inhibitors, on the consequences of traumatic brain injury in rat. Brain Res 1041:149–156.

Blois MS. 1958. Antioxidant determinations by the use of a stable free radical. Nature 181:1199–1200.

Castoldi AF, Barni S, Turin I, Gandini C, Manzo L. 2000. Early acute necrosis, delayed apoptosis and cytoskeletal breakdown in cultured cerebellar granule neurons exposed to methylmercury. J Neurosci Res 60:775–787.

Czapski GA, Cakala M, Kopczuk D, Strosznajder JB. 2004. Effect of poly (ADP-ribose) polymerase inhibitors on oxidative stress evoked hydroxyl radical level and macromolecules oxidation in cell free system of rat brain cortex. Neurosci Lett 356:45–48.

Dare E, Gotz ME, Zhivotovsky B, Manzo L, Ceccatelli S. 2000. Antioxidants J811 and 17beta-estradiol protect cerebellar granule cells from methylmercury-induced apoptotic cell death. J Neurosci Res 62:557–565.

Dare E, Gorman AM, Ahlbom E, Gotz M, Momoi T, Ceccatelli S. 2001. Apoptotic morphology does not always require caspase activity in rat cerebellar granule neurons. Neurotoxicity Res 3:501–514.

D'Amours D, Desnoyers S, Poirier GG. 1999. Poly(ADP-ribosyl)ation reactions in the regulation of nuclear functions. Biochem J 342:249–268.

Eliasson MJL, Sampei K, Mandir AS, Hurn PD, Traystman RJ, Bao J, Pieper A, Qang Z, Dawson TM, Snyder SH, Dawson VL. 1997. Poly (ADP-ribose) polymerase gene disruption renders mice resistant to cerebral ischemia. Nat Med 3:1089–1095.

Fossati S, Cipriani G, Moroni F, Chiarugi A. 2007. Neither energy collapse nor transcription underlie in vitro neurotoxicity of poly(ADP-ribose) polymerase hyper-activation. Neurochem Int 50:203–210.

Ganther HE. 1978. Modification of methylmercury toxicity and metabolism by selenium and vitamin E: possible mechanisms. Environ Health Persp 25:71–76.

Gassó S, Cristòfol RM, Selema G, Rosa R, Rodríguez-Farré E, Sanfeliu C. 2001. Antioxidant compounds and Ca^{2+} pathway blockers differentially protect against methylmercury and mercuric chloride neurotoxicity. J Neurosci Res 66:135–145.

Guo TL, Miller MA, Datar S, Shapiro IM, Shenker BJ. 1998. Inhibition of poly(ADP-ribose) polymerase rescues human T lymphocytes from methylmercury-induced apoptosis. Toxicol Appl Pharmacol 152:397–405.

Haddad M, Rhinn H, Bloquel C, Coqueran B, Szabo C, Plotkine M, Scherman D, Margaill I. 2006. Anti-inflammatory effects of PJ34, a poly(ADP-ribose) polymerase inhibitor, in transient focal cerebral ischemia in mice. Br J Pharmacol 149:23–30.

Ju BG, Lunyak VV, Perissi V, Garcia-Bassets I, Rose DW, Glass CK, Rosenfeld MG. 2006. A topoisomerase IIb-mediated dsDNA break required for regulated transcription. Science 312:1798–1803.

Kane DJ, Sarafian TA, Anton R, Hahn H, Gralla EB, Valentine JS, Ord T, Bredesen DE. 1993. Bcl-2 inhibition of neural death: decreased generation of reactive oxygen species. Science 262:1274–1277.

Kaur P, Aschner M, Syversen T. 2006. Glutathione modulation influences methyl mercury induced neurotoxicity in primary cell cultures of neurons and astrocytes. Neurotoxicology 27:492–500.

Kondo T. 1994. Total glutathione assay protocol. In: Taniguchi T, editor. Reactive oxygen species assay protocols. Tokyo: Syujun-sya. p 84–88. In Japanese.

Li J, Lin JC, Wang H, Peterson JW, Furie BC, Furie B, Booth SL, Volpe JJ, Rosenberg PA. 2003. Novel role of vitamin K in preventing oxidative injury to developing oligodendrocytes and neurons. J Neurosci 23:5816–5826.

Marty MS, Atchison WD. 1997. Pathways mediating Ca^{2+} entry in rat cerebellar granule cells following in vitro exposure to methylmercury. Toxicol Appl Pharmacol 147:319–330.

Meister A, Andersson M. 1983. Glutathione. Annu Rev Biochem 52:711–760.

Meli E, Pangallo M, Baronti R, Chiarugi A, Cozzi A, Pellegrini-Giampietro DE, Moroni F. 2003. Poly(ADP-ribose) polymerase as a key player in excitotoxicity and post-ischemic brain damage. Toxicol Lett 139:153–162.

Miller NJ, Rice-Evans C, Davies MJ, Gopinathan V, Milner A. 1993. A novel method for measuring antioxidant capacity and its application to monitoring the antioxidant status in premature neonates. Clin Sci 84:407–412.

Miura K, Imura N. 1987. Mechanism of methylmercury cytotoxicity. Crit Rev Toxicol 18:161–188.

Murphy TH, Miyamoto M, Sastre A, Schnaar RL, Coyle JT. 1989. Glutamate toxicity in a neuronal cell line involves inhibition of cystine transport leading to oxidative stress. Neuron 2:1547–1558.

Nagashima K, Fujii Y, Tsukamoto T, Nukuzuma S, Satoh M, Fujita M, Fujioka Y, Akagi H. 1996. Apoptotic process of cerebellar degeneration in experimental methylmercury intoxication of rats. Acta Neuropathol 91:72–77.

Naganuma A, Miura K, Tanaka-Kagawa T, Kitahara J, Seko Y, Toyoda H, Imura N. 1998. Overexpression of manganese-superoxide dismutase prevents methylmercury toxicity in HeLa cells. Life Sci 62:PL157–PL161.

Park ST, Lim KT, Chung YT, Kim SU. 1996. Methylmercury-induced neurotoxicity in cerebral neuron culture is blocked by antioxidants and NMDA receptor antagonists. Neurotoxicology 17:37–46.

Sakaue M, Takanaga H, Adachi T, Hara S, Kunimoto M. 2003. Selective disappearance of an axonal protein, 440-kDa ankyrin$_B$, associated with neuronal degeneration induced by methylmercury. J Neurosci Res 73:831–839.

Sakaue M, Okazaki M, Hara S. 2005. Very low levels of methylmercury induce cell death of cultured rat cerebellar neurons via calpain activation. Toxicology 213:97–106.

Sarafian T, Verity MA. 1991. Oxidative mechanisms underlying methylmercury neurotoxicity. Int J Dev Neurosci 9:147–153.

Sarafian TA, Vartavarian L, Kane DJ, Bredesen DE, Verity MA. 1994. Bcl-2 expression decreases methylmercury-induced free-radical generation and cell killing in a neural cell line. Toxicol Lett 74:149–155.

Satoh MS, Lindahl T. 1992. Role of poly(ADP-ribose) formation in DNA repair. Nature 356:356–358.

Suto MJ, Turner WR, Arundel-Suto CM, Werbel LM, Sebolt-Leopold JS. 1991. Dihydroisoquinolinones: the design and synthesis of a new series of potent inhibitors of poly(ADP-ribose) polymerase. Anti-Cancer Drug Des 7:107–117.

Suto MJ, Turner WR, Werbel LM. 1993. Substituted dihydroisoquinolinones and related compounds as potentiators of the lethal effects of radiation and certain chemotherapeutic agents; selected compounds, analogs and process. United States Patent 5:177,075.

Takahashi K, Pieper A, Croul SE, Zhang J, Snyder S, Greenberg JH. 1999. Post-treatment with an inhibitor of poly(ADP-ribose) polymerase attenuates cerebral damage in focal ischemia. Brain Res 829:46–54.

Tanaka S, Takehashi M, Iida S, Kitajima T, Kamanaka Y, Stedeford T, Banasik M, Ueda K. 2005. Mitochondrial impairment induced by poly (ADP-ribose) polymerase-1 activation in cortical neurons after oxygen and glucose deprivation. J Neurochem 95:179–190.

Ying W, Alano CC, Garnier P, Swanson RA. 2005. NAD^+ as a metabolic link between DNA damage and cell death. J Neurosci Res 79:216–223.

Zhang Y, Rosenberg PA. 2004. Caspase-1 and poly(ADP-ribose) polymerase inhibitors may protect against peroxynitrite-induced neurotoxicity independent of their enzyme inhibitor activity. Eur J Neurosci 20:1727–1736.

BRAIN RESEARCH 1273 (2009) 155–162

available at www.sciencedirect.com

ScienceDirect

www.elsevier.com/locate/brainres

BRAIN RESEARCH

Research Report

Acceleration of methylmercury-induced cell death of rat cerebellar neurons by brain-derived neurotrophic factor in vitro

Motoharu Sakaue[a,b,*], *Naoko Mori*[b], *Misato Makita*[b], *Kana Fujishima*[b], *Shuntaro Hara*[c], *Kazuyoshi Arishima*[a], *Masako Yamamoto*[a]

[a]*Department of Anatomy II, School of Veterinary Medicine, Azabu University, 1-17-71 Fuchinobe, Sagamihara 229-8501, Japan*
[b]*Department of Public Health and Molecular Toxicology, School of Pharmaceutical Sciences, Kitasato University, 5-9-1 Shirokane, Minato-ku, Tokyo 108-8641, Japan*
[c]*Department of Health Chemistry, School of Pharmaceutical Sciences, Showa University, 1-5-8 Hatanodai, Shinagawa-ku, Tokyo 142-8555, Japan*

ARTICLE INFO

Article history:
Accepted 15 March 2009
Available online 28 March 2009

Keywords:
TrkB
BDNF
NT-4
B35 cell line
Methylmercury
Primary culture

ABSTRACT

Brain-derived neurotrophic factor (BDNF) is a member of the nerve growth factor (NGF) family and has been shown to promote neuronal survival and contribute to neural development. Although methylmercury, a neurotoxin, induces the cell death of neurons in vitro, there is little information regarding the effects of neurotrophins on the methylmercury-induced cell death of neurons. In the present study, we investigated the effect of BDNF on methylmercury-induced cell death in a primary culture of rat cerebellar granular cells. BDNF increased the viability of the cultured cells when treated alone, but unexpectedly accelerated the cell death induced by administration of methylmercury. Among other growth factors tested, only neurotrophin-4 (NT-4) demonstrated a similar acceleration of methylmercury-induced cell death. The cell death-accelerating effect of BDNF was inhibited by a BDNF-neutralizing antibody or a MAPK inhibitor. To determine whether the effect of BDNF occurs via TrkB, a receptor of BDNF and NT-4, we investigated the effects of BDNF and methylmercury in a TrkB transformant of rat neuroblastoma B35 cells. The methylmercury-induced cell death of the TrkB transformant was accelerated by BDNF, while that of the mock transformant was not. These results indicate that BDNF accelerates methylmercury-induced cell death via TrkB, at least in vitro, and suggest that BDNF and TrkB may also contribute to the sensitivity of neurons to methylmercury toxicity.

1. Introduction

The neurotrophin family, which includes nerve growth factor (NGF), brain-derived neurotrophic factor (BDNF), neurotrophin-3 (NT-3), and neurotrophin-4/5 (NT-4/5), regulates the survival and functions of central and peripheral neurons (Snider, 1994). BDNF has been well investigated with regard to these functions and regulations in the central

* *Corresponding author*. Department of Anatomy II, School of Veterinary Medicine, Azabu University, 1-17-71 Fuchinobe, Sagamihara 229-8501, Japan. Fax: +81 42 769 1620.
E-mail address: sakaue@azabu-u.ac.jp (M. Sakaue).

0006-8993/$ – see front matter
doi:10.1016/j.brainres.2009.03.035

nervous system, and has been shown to confer protection against various types of neuronal cell death, including serum-deprived, excitotoxic, and oxidative stress-mediated death. Neural cells secrete BDNF to serve as a paracrine or endocrine factor for the survival of neurons and for maintenance of neural normal function. The effects of BDNF are mediated by its binding to tropomyosin-related kinase (Trk) B, a neurotrophin receptor, with high affinity, after which TrkB processes signal transduction through primarily three signaling pathways—the mitogen-activated protein kinase (MAPK), the phospholipase C (PLC) γ, and the phosphoinositide 3-kinase (PI3K) pathway. TrkB binds not only BDNF, but also NT-4/5 with high affinity and NT-3 with lesser affinity. In contrast, TrkA binds NGF and TrkC binds NT-3 specifically, after which both these Trks process signal transduction in the same manner as TrkB (for review, see Bibel and Barde, 2000; Reichardt, 2006) in order to realize the neurotrophic effects. Phenotypic analysis in BDNF- or TrkB-null mice has revealed that BDNF and TrkB are essential for normal brain development (Snider, 1994). Furthermore, even in adults, BDNF plays an important role as a modulator in synaptic development and plasticity in learning and memory.

Methylmercury is well known as a neurotoxicant. Methylmercury toxicity involves disruption of intracellular homeostasis with, for example, increases in intracellular calcium (Ca^{2+}) concentrations, reactive oxygen species production and extracellular concentration of glutamate via inhibition of glutamate uptake of astrocytes (Sarafian and Verity, 1991; Aschner et al., 1993; Marty and Atchison, 1997; Sakaue et al., 2005). Cerebellar granule cells, which are particularly vulnerable to methylmercury-induced damage in vivo, have provided a good model for analysis of methylmercury-induced neuronal cell death in vitro (Dare et al., 2000; Castoldi et al., 2000). We have previously investigated the mechanisms of methylmercury toxicity and screened growth factors and chemicals in order to identify those that confer protection against methylmercury (Sakaue et al., 2005; 2006; 2008). In the present study, we continued this investigation by examining whether BDNF, which has been shown to protect against some types of cell death, would also protect against methylmercury-induced cell death in a primary culture of rat cerebellar granular cells. Our results unexpectedly demonstrated that BDNF accelerates methylmercury-induced cell death. To investigate the possible mechanism of this effect, we used a stable transformant of TrkB in rat neuroblastoma B35 cells, and showed that TrkB was involved in the acceleration of methylmercury-induced cell death by BDNF.

2. Results

2.1. BDNF increases methylmercury-induced cell death of rat cerebellar granule cells

To examine the effects of BDNF on the neurotoxicity of methylmercury, we measured the viability of rat cerebellar granule cells after treatment of BDNF, methylmercury, or both, expecting that BDNF would exhibit a neurotrophic action. Treatment with methylmercury alone significantly decreased the viability of the cells to approximately 70% of that of non-treated cells ($p=0.002$; Figs. 1B and E). Treatment with BDNF alone significantly increased the viability of the cells to approximately 115% of that of non-treated cells ($p<0.001$). However, co-treatment with BDNF and methylmercury further decreased the viability of the cells to 50.4%, which was significantly lower than the viability of the methylmercury-treated cells ($p=0.009$). Both the increase and decrease of the cell viability occurred in a BDNF concentration-dependent manner (Figs. 1D and E). In addition, co-treatment with BDNF and methylmercury had different effects on the cell viability depending on whether the incubation time was 24 h or 48 h. At 24 h of incubation, the viability of cells co-treated with BDNF and methylmercury was 103%, significantly greater than the 96% viability of cells treated with methylmercury alone ($p=0.009$). Conversely, at 48 h of incubation, the viability of co-treated cells was 47.8%, significantly smaller than the 69% viability of methylmercury-treated cells ($p<0.001$). Thus the accelerating effect of BDNF on the methylmercury-induced cell death appeared only after incubation for 24 h, increased between 24 h and 48 h of incubation, and was slightly but not significantly apparent after incubation for 36 h ($p=0.065$; methylmercury-treated versus co-treated cells) (Fig. 1F). Therefore these results indicate that BDNF functions as an accelerator of cell death after methylmercury cytotoxicity begins to appear in primary cultured cells, but not before.

NT-4 is another ligand of TrkB (Bibel and Barde, 2000; Reichardt, 2006). Accordingly, we next examined whether NT-4 also accelerates methylmercury-induced cell death. When administered singly, NT-4 at 100 ng/ml significantly increased cell viability to 115% compared with control cells ($p=0.01$). However, the viability of cells co-treated with methylmercury and NT-4 was significantly decreased compared to the viability of treated with methylmercury alone (Fig. 1G; $p=0.004$). This effect of NT-4 on methylmercury-induced cell death occurred in a concentration-dependent manner. The percentages of viable NT-4-treated, methylmercury-treated, and NT-4/methylmercury co-treated cells were 115%, 69%, and

Fig. 1 – BDNF accelerates methylmercury-induced cell death in a primary culture of rat cerebellar granule cells. (A–D) Phase-contrast micrographs of cerebellar granular cells in BDNF-treated culture. The microphotographs show (A) control, (B) methylmercury-treated (30 nM), (C) BDNF-treated (100 ng/ml), and (D) methylmercury and BDNF-treated (30 nM and 100 ng/ml) cells. Bar=50 μm. Cerebellar granule cell viability was assayed 48 h after treatment with methylmercury (30 nM) and/or with the neurotrophins (E and F) BDNF, (G) NT-4, or (H) NGFβ. (F) Alteration of the BDNF effect at 100 ng/ml on the cell viability over time. Data are expressed as the mean±S.D. (E, G, H, $n=3$; F, $n=4$) of the percentage of cell viability compared to the group without methylmercury and BDNF treatments. Statistical analyses were performed using two-way ANOVA with Fisher's PLSD test as a post-hoc test. *, a, b, c, and d denote significant differences between different letters ($p<0.05$).

55%, respectively. This result indicates that NT-4 accelerated methylmercury-induced cell death in a manner similar to BDNF, and suggests that TrkB is involved in the mechanism of the BDNF effect. Finally, because NGFβ also has the ability to bind to TrkA, we examined whether NGFβ had any effect on methylmercury-induced cell death. However, treatment of cerebellar neurons with NGFβ and methylmercury did not significantly alter the viability of cells compared with

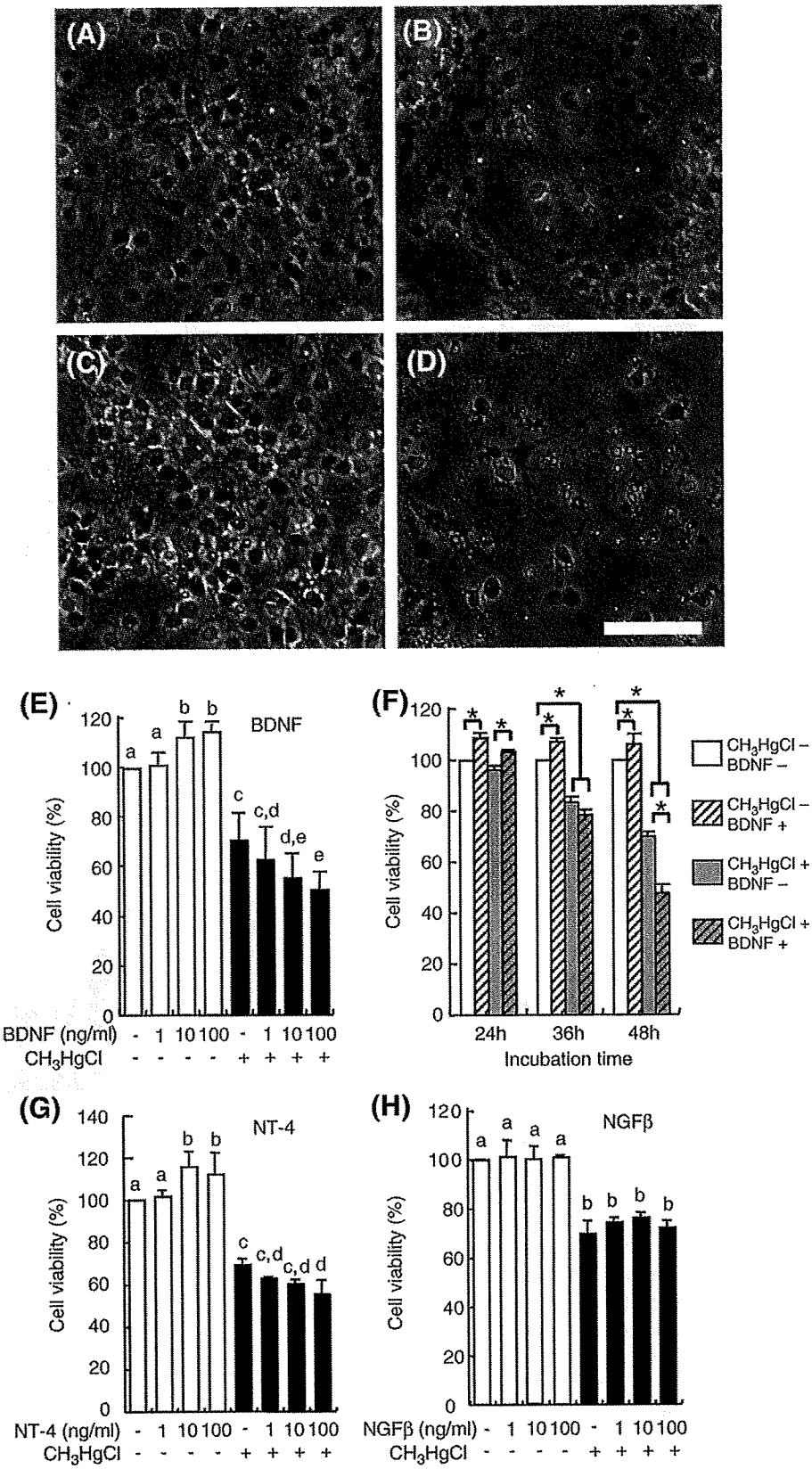

treatment by methylmercury alone ($p=0.441$), and in fact, treatment with NGFβ alone did not induce a significant change in viability compared with the non-treated control cells (Fig. 1H; $p=0.753$).

2.2. *The acceleration of the cell death by BDNF involves its binding to TrkB and MAP signal transduction*

BDNF and NT-4 bind to TrkB and activate it, which initiates signal transductions. To clarify whether BDNF binding to TrkB and activation of the signal transduction of MAP are involved in the effect of BDNF, we elucidated the effects of a BDNF-neutralizing antibody and MAPK inhibitor on the acceleration of methylmercury-induced cell death by BDNF. As shown in Fig. 2A, the viability of the cells co-treated with methylmercury and BDNF was 46%, and that of the cells co-treated with plus BDNF-neutralizing antibody was 64%, which indicates that the treatment with the BDNF-neutralizing antibody significantly suppressed the BDNF-induced acceleration of cell death. This suppression was in a concentration-dependent manner of the antibody ($p<0.001$, methylmercury/BDNF co-treated versus plus the neutralizing antibody co-treated cells).

A MAPK inhibitor, U0126, suppressed the cell death induced by co-treatment with methylmercury and BDNF or by treatment with only methylmercury (Fig. 2B). These results indicate that the MAPK inhibitor inhibited not only the accelerating effect of BDNF on methylmercury-induced cell death, but also the cell death induced by methylmercury alone. The cell viability of the cells co-treated with methylmercury, BDNF, and the MAPK inhibitor, tended to be lower than the cell viability of BDNF-treated cells, which suggests that U0126 prevented BDNF from acting as an accelerator and a neurotrophic factor by inhibiting the MAPK pathway. Furthermore, to examine the mRNA expression of the neurotrophin receptors, TrkA, TrkB, and TrkC, total RNAs from the primary cultured cerebellar cells and from the cerebrum as a positive control were subjected to RT-PCR. mRNA expression of all Trks was detected in the cerebrum. However, only TrkB mRNA was intensively expressed among receptors in the primarily cultured cerebellar cells, while mRNA expression of TrkA and TrkC was not observed (Fig. 2C).

To examine whether TrkB is involved in the effect of BDNF on methylmercury cytotoxicity, we performed experiments using a stable transformant for TrkB (Fig. 3). BDNF significantly increased the viability of the TrkB transformant cells, to 135%, but not that of the mock transformant cells. These effects indicate that the over-expressed TrkB protein can function normally in TrkB-transformant cells, and that BDNF has a neurotrophic effect on the TrkB-transformant cells through TrkB. In the group treated with 150 nM methylmercury, the viability was similar between the both trans-

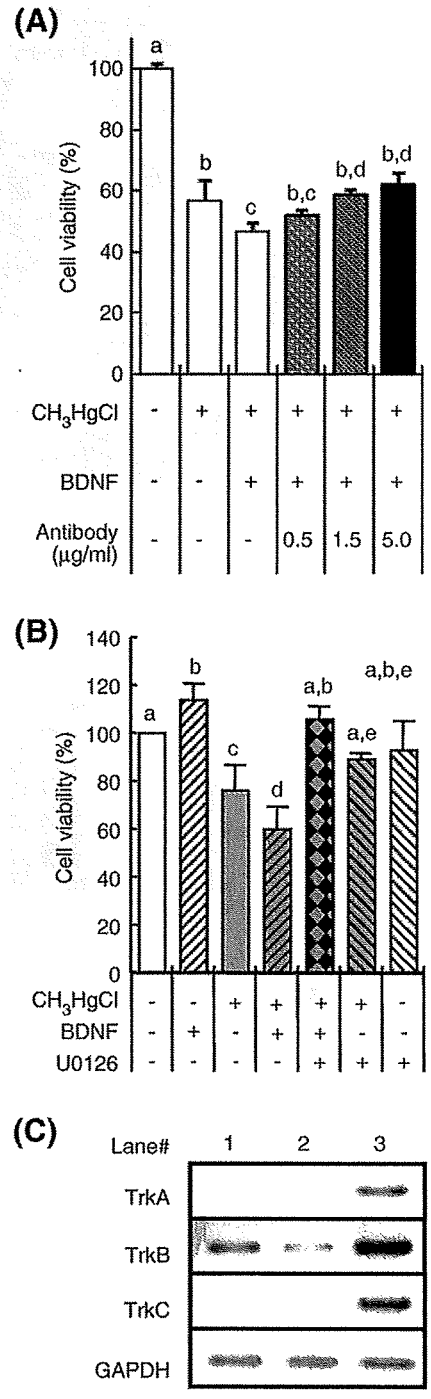

Fig. 2 – Involvement of TrkB and its signal cascade in the acceleration of methylmercury-induced cell death by BDNF treatment (10 ng/ml). Cell viability was assayed 48 h after methylmercury treatment at 30 nM. (A) Inhibitory effect of the neutralizing antibody against BDNF and (B) inhibitory effect of the MAPK inhibitor, U0126 (30 μM) on the augmentation of cell death by BDNF. (A and B) Data are expressed as the mean±S.D. (A, $n=4$; B, $n=3$) of the percentage of cell viability compared to the group without methylmercury and BDNF treatments. Statistical analyses were performed using two-way ANOVA with Fisher's PLSD test as a post-hoc test. a, b, c, d, and e denote significant differences between different letters ($p<0.05$). (C) RT-PCR analysis of the mRNA expression of neurotrophin receptors in a primary culture of rat cerebellar granule cells (lanes #1 and 2) and cerebrum (lane #3). The cDNAs for the PCR templates were synthesized from total RNA that was independently prepared from the primary cultures of rat cerebellar granule cells or the whole cerebrum of an adult rat.

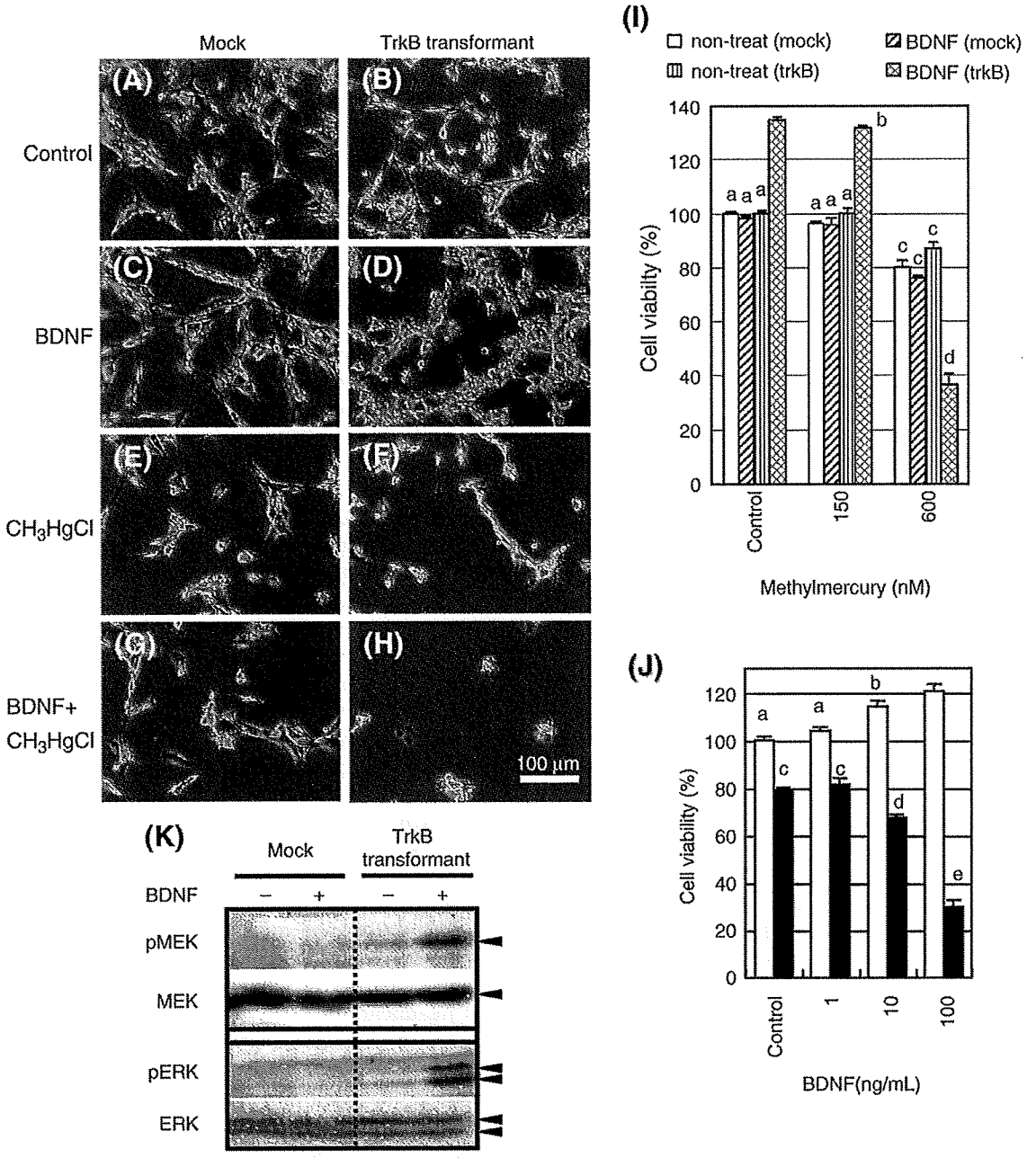

Fig. 3 – TrkB expression is necessary for BDNF to act as an accelerator for methylmercury-induced cell death in the stable transformant of the TrkB expression vector. The cells, mock (A, C, E, G) and TrkB (B, D, F, H) transformants, were incubated and then fixed 40 h after methylmercury treatment. Phase-contrast micrographs show the results in (A, B) control, (C, D) BDNF-treated, (E, F) CH_3HgCl-treated, (G, H) or BDNF plus CH_3HgCl-treated cells. (I) Viability of the stable transformant 40 h after treatment. The concentration of BDNF is 100 ng/ml. Bar=100 μm. (J) BDNF alters the viability of the TrkB transformant cells in a dose-dependent manner. The TrkB transformant cells were incubated with methylmercury at 0 nM (white bar) or 600 nM (black bar). Data are expressed as the mean±S.D. ($n=3$) of the percentage of cell viability to mock control at (I) or to control treated with 0 nM of methylmercury at (J). Statistical analyses were performed using two-way ANOVA with Fisher's PLSD test as a post-hoc test. a, b, c, d, and e denote significant differences between different letters ($p<0.05$). (K) Detection of phosphorylated ERK (pERK) and MEK (pMEK) to confirm the function of the expressed TrkB in the mock or TrkB transformants with (+) or without (–) BDNF treatment. Cell lysates were subjected to Western blotting, and the results were confirmed with anti-pERK, anti-ERK, anti-pMEK or anti-MEK antibodies.

formants. In contrast, in the cells treated with 600 nM methylmercury, the cell viabilities of both transformants significantly decreased to approximately 80%. Only the viability of the TrkB-transformant cells treated with BDNF fell further, to 38% (Fig. 3I; $p<0.001$; 600 nM methylmercury-treated versus plus BDNF-treated cells of TrkB-transformant).

This effect in the TrkB-transformant cells was dependent on the dose of BDNF (Fig. 3J). Western blot analysis showed that two signal-transduction factors in a TrkB down-stream, extracellular signal-regulated kinase (ERK) and MAPK/ERK kinase (MEK), were phosphorylated by BDNF treatment in the TrkB transformant, but not in the mock transformant cells (Fig. 3K), which demonstrates that the TrkB transformant has a normally functioning TrkB protein, while the mock transformant does not. These results indicate that TrkB is necessary for the acceleration of methylmercury-induced cell death or for the increase of cell viability through BDNF treatment.

3. Discussion

This is the first study documenting that BDNF aggravates the neuronal death induced by an environmental toxin, methylmercury, although BDNF is included in the NGF family. We demonstrated that BDNF and NT-4 accelerate the methylmercury-induced cell death of rat cerebellar granule cells in primary cultures in a dose-dependent manner, but that NGFβ does not, which is supported by the evidence that primary cultured cells expressed a high level of TrkB but not TrkA mRNA, because the neurotrophins need to bind to specific receptors in order to achieve their cell death-accelerating effects (Bibel and Barde, 2000; Reichardt, 2006). The experiment using a neutralizing antibody against BDNF also proved the necessity of BDNF binding to TrkB for the effect of BDNF as an accelerator of methylmercury-induced cell death. Furthermore, the methylmercury-induced death in the TrkB transformant of rat neuroblastoma cell line B35 was accelerated by BDNF treatment, but not that in the mock transformant. These results indicate that TrkB activation by BDNF is responsible for the accelerating effect on methylmercury-induced cell death. Among Trks, the cells of the primary culture expressed only TrkB in the present study. Therefore, as TrkB is a receptor of BDNF, only BDNF should have been an accelerating factor against methylmercury-induced cell death among neurotrophins. Had TrkA or TrkC been expressed in the primary culture, NGF or NT-3 might have induced an acceleration of methylmercury-induced cell death, because TrkA and TrkC can process signal transduction through at least three signaling pathways, MAPK, PLC γ, and PI3K, that TrkB also processes (Bibel and Barde, 2000; Reichardt, 2006). However, the results of the present study did not sufficiently clarify whether TrkA and TrkC are involved in the accelerating effect on methylmercury-induced cell death in the manner of TrkB. To resolve these questions, more experiments will be needed to observe the effects of NGFβ on methylmercury-induced death in TrkA-expressing cells, such as rat adrenal pheochromocytoma PC-12 cells.

When the cytotoxicity of methylmercury did not appear, BDNF functioned as a neurotrophin for both the primary cultured neurons of the cerebellum and the TrkB transformant of B35 cells co-treated with methylmercury and BDNF. However, when the cell viability was decreased by methylmercury toxicity, BDNF functioned as an accelerator of the methylmercury-induce cell death (Figs. 1 and 3). These results indicate that BDNF exhibits not only trophic activity, but also death acceleration activity, and thus that the role of BDNF is altered by the appearance of methylmercury cytotoxicity.

There may be cross-talk mechanisms between the BDNF and methylmercury pathways. In primary cultured neurons from mice cerebella, methylmercury shows its neurotoxicity by increases in intracellular Ca^{2+} concentrations through NMDA receptor activation, and the toxicity is suppressed with NMDA receptor antagonists (Park et al., 1996). The disappearance of methylmercury neurotoxicity by treatment with NMDA receptor antagonists has also been observed in an in vivo study (Miyamoto et al., 2001). Using the same culture system used in the present study, we previously showed that methylmercury induces an increase in intracellular Ca^{2+} concentrations, which in turn activates calpain, a Ca^{2+} concentration-dependent protease, to play its role in methylmercury-induced cell death (Sakaue et al., 2005). BDNF phosphorylates NMDA receptors via TrkB, resulting in a slight increase in intracellular Ca^{2+} concentrations, but the levels of intracellular Ca^{2+} concentrations should still be low compared to the levels of intracellular Ca^{2+} concentrations increased by methylmercury. This BDNF effect on the intracellular Ca^{2+} concentrations is suppressed by treatment with a kinase inhibitor against Trks, K-252a, or an NMDA receptor antagonist, MK-801 (Xu et al., 2006; Sanchez-Perez et al., 2006). As shown above, U0126 also inhibited the effects of methylmercury and BDNF (Fig. 2B). Moreover, we determined that a subtype of the NMDA receptor, NR1, is phosphorylated by BDNF or NT-4 treatment, but not by NT-3 in our primary culture system (data not shown). Thus, BDNF might realize its acceleration of methylmercury-induced cell death by stimulating a methylmercury-induced increase of intracellular Ca^{2+} concentration. However, confirmation of this proposed mechanism is beyond the scope of the present study. Further studies using Ca^{2+} indicators or endogenous markers for increases in Ca^{2+} concentrations will be needed in order to detect any augmentation of intracellular Ca^{2+} concentrations by BDNF treatment.

In conclusion, the present results indicate that BDNF exacerbates methylmercury-induced cell death via TrkB, indicating that BDNF and TrkB are factors regulating the sensitivity to methylmercury cytotoxicity. The neurotoxicity of methylmercury has at least two toxicological characteristics, as follows. First, fetuses and infants show a higher sensitivity to methylmercury than adults (Takeuchi, 1968; Bakir et al., 1973; Harada, 1968; Marsh et al., 1980). BDNF is indispensable for the development of normal structures, as well as for cell survival and function, in the nerve tissue of developing animals such as fetuses and infants (Sinder, 1994; Bibel and Barde, 2000). If the effect of BDNF as an accelerator, not as a neurotrophin, on the methylmercury-induced cell death in vitro is also detected in the brain, the indispensability of BDNF for normal development of nerve tissue might determine the higher sensitivity to methylmercury in developing animals. The second characteristic is that neurons highly sensitive to methylmercury toxicity, such as cerebellar granular cells and granular cells of the cerebral cortex, are in particular areas of the central nervous system (Tsubaki and Irukayama, 1977; Weiss et al., 2002), which means that the difference in sensitivity to methylmercury occurs between neurons even in the same brain. In the present study, BDNF

promoted methylmercury-induced death of TrkB-expressing cells, suggesting that neurons which express TrkB will be more sensitive to methylmercury than those which do not. Thus, the difference in methylmercury sensitivity between neurons in the brain may be determined by whether or not individual neurons express TrkB. And in fact, the second to fifth layers of the cerebral cortex of humans show higher levels of TrkB mRNA, while the second and following layers show a higher expression of BDNF mRNA (Webster et al., 2006), which is in partial agreement with the layers of the human cerebral cortex that are degenerated by methylmercury exposure, particularly the second and third layers (Takeuchi et al., 1977). The BDNF-induced acceleration of methylmercury-induced cell death is a good model to clarify the mechanisms of this BDNF effect. Further investigation using this model may help to identify the mechanisms and characteristics of methylmercury toxicity.

4. Experimental procedures

4.1. *Cell cultures and treatment*

Primary cultures of cerebellar granule neurons were prepared from Wistar rats (Jcl:Wistar; Clea Co., Tokyo, Japan) within 24 h after birth, as described previously (Sakaue et al., 2005). Briefly, cerebella were removed from the pups and incubated with trypsin for 13 min at room temperature were minced by mild triturating with a Pasteur pipette. Cerebellar granule cells were seeded in Eagle's minimal essential medium (Gibco BRL, Grand Island, NY) containing 1 mg/ml BSA, 10 μg/ml bovine insulin, 0.1 nM thyroxin, 0.1 μg/mg human transferrin, 1 μg/ml aprotinin, 30 nM Na_2SeO_3, 0.25% glucose, 100 U/mL penicillin, and 135 μg/mL streptomycin on poly-L-lysine-coated dishes and cultured for 2 days. Rat neuroblastoma B35 cells were purchased from the American Type Culture Collection (ATCC, Manassas, VA). The B35 cells were cultured in growth medium, Dulbecco's modified Eagle's medium supplemented with 10% fetal calf serum (HyClone, South Logan, UT), 100 U/mL penicillin, and 135 μg/mL streptomycin. The medium was changed every second day. These cell culture supplements were purchased from Sigma-Aldrich (St. Louis, MO).

The cells were pre-incubated for 24 h and treated with methylmercuric chloride (Tokyo Kasei Kogyo. Co., Ltd., Tokyo, Japan) at the concentrations indicated in the figures with or without recombinant human BDNF (Peprotech, London, UK), recombinant human neurotorophin-4 (NT-4; Sigma-Aldrich), or mouse nerve growth factor (NGFβ; Sigma-Aldrich). These neurotrophins were added to the medium 30 min before the methylmercury treatment. In addition, a BDNF-neutralizing antibody (Sigma-Aldrich) and a MAPK inhibitor, U0126 (Calbiochem, Darmstadt, Germany), were used to investigate whether the BDNF effect involves the binding of BDNF to its receptor and activation of the MAP signaling cascade. The numbers of viable cells of the primary culture and the B35 cell line were estimated by crystal violet staining, as described previously (Sakaue et al., 2005). All experiments were carried out in accordance with the Kitasato University Guidelines for Animal Care and Experimentation.

4.2. *Cloning of the stable transformant of B35 cells expressing TrkB*

Using two primers, rTrkB1FEcoRI (5′-GAATTCCTGGCGTATAGG-AC-3′) and rTrkB1RNotI (5′-GCGGCCGCACTGTCAGAGCGAA-3′), designated on the sequences of rat TrkB from GenBank (Accession No. NM_012731), rat TrkB cDNA was amplified with rat brain cDNA as a template. An approximately 2.8-kb cDNA fragment of TrkB was cloned into the EcoRI/NotI site of pcDNA3.1 (Invitrogen, Carlsbad, CA) for construction of the expression plasmid and then sequenced.

B35 cells were transfected with the TrkB expression construct using Lipofectamin (Invitrogen, Carlsbad, CA) according to the manufacturer's instructions. Stable transformants were selected in growth medium containing 0.8 mg/ml geneticin (G418; Invitrogen). G418-resistant cells were cloned, and the TrkB mRNA expression was checked in each clone using RT-PCR. To confirm the function of the expressed TrkB protein in the transformant, phosphorylation of two factors of signal transduction in the region down-stream of TrkB, ERK and MEK, in the selected clone in mock or TrkB transformants after BDNF treatment was detected using Western blot analysis, which was performed as described in our previous report (Sakaue et al., 2005). Briefly, after BDNF treatment at 50 ng/ml, B35 cells were washed three times with PBS (pH 7.4) and harvested in Lamini's buffer (3% SDS, 62.5 mM Tris base, pH 6.8). The protein concentration in cell lysates was determined by a BCA assay (Bio-Rad, Hercules, CA). SDS-polyacrylamide gel electrophoresis (PAGE) was performed with 50 μg of lysate protein. For Western blotting, proteins were transferred to a PVDF membrane (GE Healthcare, Buckinghamshire, UK) at 100 V for 2 h. To determine the phosphorylation state, the membrane was washed in 0.05% Tween-20 PBS (T-PBS) and incubated in a blocking buffer, 1% bovine serum albumin T-PBS, for 1 h at room temperature. Then, the first antibody, i.e., rabbit anti-phospho-ERK (pERK) 1/2 antibody, anti-ERK1/2 antibody, anti-phospho-MEK antibody or anti-MEK antibody, was reacted with the membrane for 12 h at 4 °C, followed by reaction with horseradish peroxidase-conjugated secondary antibody (1:1000; Sigma) for 1 h at 4 °C. These antibodies were purchased from Cell Signaling Technology, Inc. (Danvers, MA). Enhanced chemiluminescence by Chemilumi one (Nacali Tesque, Kyoto, Japan) was determined by exposure to an X-ray film (GE Healthcare).

4.3. RT-PCR

Total RNAs of rat cerebellar neuronal culture and whole cerebella were extracted and reverse-transcribed in a reaction solution containing SuperScript™ II reverse transcriptase and Oligo$(dT)_{12-18}$Primer (Invitrogen) for producing cDNA, as described previously (Sakaue et al., 2002). The cDNAs were stocked at −20 °C before use. PCRs for TrkA, TrkB, and TrkC were carried out in 50 μl of PCR mixture containing 1.25 U of ExTaq™ polymerase (Takara Biochemicals, Otsu, Japan), 1×ExTaq™ buffer, 0.2 mM dNTP mixture, 100 pM of each primer, and 2 μl of the cDNA. The PCR conditions for all genes were as follows: an initial denaturation step at 95 °C for 3 min, followed by 40 cycles of denaturation at 95 °C for 30 s, annealing at 60 °C for 30 s, and extension at 72 °C for 45 s, with

a final extension step at 72 °C for 3 min. The primer sequences of the neurotrophin receptors reported by Nemoto et al. (2000) were referenced in the present study.

Acknowledgments

This study was supported by a grant (no. 20780221, to MS) from the Ministry of Education, Culture, Sports, Science, and Technology of Japan, by a project grant (Young Scientist Research Training Award, 2008) from the Azabu University Research Services Division (to MS), and by a grant from The Morinaga Foundation for Health and Nutrition (to MS).

REFERENCES

Aschner, M., Du, Y.L., Kimelberg, H.K., 1993. Methylmercury-induced alterations in excitatory amino acid transport in rat primary astrocyte cultures. Brain Res. 602, 181–186.

Bakir, F., Damluji, S.F., Amin-Zaki, L., Murtadha, M., Khalidi, A., al-Rawi, N.Y., Tikriti, S., Dahahir, H.I., Clarkson, T.W., Smith, J.C., Doherty, R.A., 1973. Methylmercury poisoning in Iraq. Science 191, 230–241.

Bibel, M., Barde, Y.A., 2000. Neurotrophins: key regulators of cell fate and cell shape in the vertebrate nervous system. Genes Dev. 14, 2919–2937.

Castoldi, A.F., Barni, S., Turin, I., Gandini, C., Manzo, L., 2000. Early acute necrosis, delayed apoptosis and cytoskeletal breakdown in cultured cerebellar granule neurons exposed to methylmercury. J. Neurosci. Res. 60, 775–787.

Dare, E., Gotz, M.E., Zhivotovsky, B., Manzo, L., Ceccatelli, S., 2000. Antioxidants J811 and 17beta-estradiol protect cerebellar granule cells from methylmercury-induced apoptotic cell death. J. Neurosci. Res. 62, 557–565.

Harada, Y., 1968. Congenital (or fetal) Minamata disease. Minamata Disease. Kumamoto University, Kumamoto, pp. 93–118.

Marsh, D.O., Myers, G.J., Clarkson, T.W., Amin-Zaki, L., Tikriti, L., Majeed, M.A., 1980. Fetal methylmercury poisoning: clinical and toxicological data on 29 cases. Ann. Neurol. 7, 348–353.

Marty, M.S., Atchison, W.D., 1997. Pathways mediating Ca^{2+} entry in rat cerebellar granule cells following in vitro exposure to methylmercury. Toxicol. Appl. Pharmacol. 147, 319–330.

Miyamoto, K., Nakanishi, H., Moriguchi, S., Fukuyama, N., Eto, K., Wakamiya, J., Murao, K., Arimura, K., Osame, M., 2001. Involvement of enhanced sensitivity of N-methyl-D-aspartate receptors in vulnerability of developing cortical neurons to methylmercury neurotoxicity. Brain. Res. 901, 252–258.

Nemoto, K., Miyata, S., Nemoto, F., Yasumoto, T., Murai, U., Kageyama, H., Degawa, M., 2000. Gene expression of neurotrophins and their receptors in lead nitrate-induced rat liver hyperplasia. Biochem. Biophys. Res. Commun. 275, 472–476.

Park, S.T., Lim, K.T., Chung, Y.T., Kim, S.U., 1996. Methylmercury-induced neurotoxicity in cerebral neuron culture is blocked by antioxidants and NMDA receptor antagonists. Neurotoxicol. 17, 37–46.

Reichardt, L.F., 2006. Neurotrophin-regulated signaling pathways. Phil. Trans. R. Soc. B 361, 1545–1564.

Sakaue, M., Ishimura, R., Kurosawa, S., Fukuzawa, N.H., Kurohmaru, M., Hayashi, Y., Tohyama, C., Ohsako, S., 2002. Administration of estradiol-3-benzoate down-regulates the expression of testicular steroidogenic enzyme genes for testosterone production in the adult rat. J. Vet. Med. Sci. 64, 107–113.

Sakaue, M., Okazaki, M., Hara, S., 2005. Very low levels of methylmercury induce cell death of cultured rat cerebellar neurons via calpain activation. Toxicology 213, 97–106.

Sakaue, M., Adachi, T., Okazaki, M., Nakamura, H., Mori, N., Hara, S., Sakabe, K., 2006. Effects of sodium selenite on methylmercury-induced cell death and on mercury accumulation in rat cerebellar neurons in primary culture. Bull. Environ. Contam. Toxicol. 77, 779–784.

Sakaue, M., Mori, N., Okazaki, M., Ishii, M., Inagaki, Y., Iino, Y., Miyahara, K., Yamamoto, M., Kumagai, T., Hara, S., Yamamoto, M., Arishima, K., 2008. Involvement of independent mechanism upon poly(ADP-ribose) polymerase (PARP) activation in methylmercury cytotoxicity in rat cerebellar granule cell culture. J. Neurosci. Res. 86, 3427–3434.

Sanchez-Perez, A.M., Llansola, M., Felipo, V., 2006. Modulation of NMDA receptors by AKT kinase. Neurochem. Inter. 49, 351–358.

Sarafian, T., Verity, M.A., 1991. Oxidative mechanisms underlying methylmercury neurotoxicity. Int. J. Dev. Neurosci. 9, 147–153.

Sinder, W.D., 1994. Functions of the neurotrophins during nervous system development: what the knockouts are teaching us. Cell 77, 627–638.

Takeuchi, T., 1968. Pathology of Minamata disease. Minamata Disease. Kumamoto University, Kumamoto, pp. 141–228.

Webster, M.J., Herman, M.M., Kleinman, J.E., Weickert, C.S., 2006. BDNF and trkB mRNA expression in the hippocampus and temporal cortex during the human lifespan. Gene Expression Patterns 6, 941–951.

Weiss, B., Clarkson, T.W., Simon, W., 2002. Silent latency periods in methylmercury poisoning and in neurodegenerative disease. Env. Health Perspect. 110 (suppl 5), 851–854.

Xu, F., Plummer, M.R., Len, G.W., Nakazawa, T., Yamamoto, T., Black, I.B., Wu, K., 2006. Brain-derived neurotrophic factor rapidly increases NMDA receptor channel activity through Fyn-mediated phosphorylation. Brain Res. 1121, 22–34.

BJ www.biochemj.org

Biochem. J. (2010) 425, 361–371 (Printed in Great Britain) doi:10.1042/BJ20090045

online data

Microsomal prostaglandin E synthase-1 in both cancer cells and hosts contributes to tumour growth, invasion and metastasis

Daisuke KAMEI*†, Makoto MURAKAMI*‡§, Yuka SASAKI*, Yoshihito NAKATANI*, Masataka MAJIMA‖, Yukio ISHIKAWA¶, Toshiharu ISHII¶, Satoshi UEMATSU**, Shizuo AKIRA**, Shuntaro HARA*[1] and Ichiro KUDO*[2]

*The Department of Health Chemistry, School of Pharmacy, Showa University, 1-5-8 Hatanodai, Shinagawa-ku, Tokyo 142-8555, Japan, †Department of Research and Development for Innovative Medical Needs, School of Pharmacy, Showa University, 1-5-8 Hatanodai, Shinagawa-ku, Tokyo 142-8555, Japan, ‡Tokyo Metropolitan Institute of Medical Science, 2-1-6 Kamikitazawa, Setagaya-ku, Tokyo 156-8506, Japan, §PRESTO, Japan Science and Technology Agency, 4-1-8 Honcho Kawaguchi, Saitama 332-0012, Japan, ‖Department of Pharmacology, School of Medicine, Kitasato University, 1-15-1 Kitasato, Sagamihara, Kanagawa 228-8555, Japan, ¶Department of Pathology, School of Medicine, Toho University, 5-21-16 Omori-Nishi, Ohta-ku, Tokyo 143-8540, Japan, and **Department of Host Defense, Research Institute for Microbial Diseases, Osaka University, 3-1 Yamada-oka, Suita, Osaka 565-0871, Japan

mPGES-1 (microsomal prostaglandin E synthase-1) is a stimulus-inducible enzyme that functions downstream of COX (cyclo-oxygenase)-2 in the PGE_2 (prostaglandin E_2)-biosynthesis pathway. Although COX-2-derived PGE_2 is known to play a role in the development of various tumours, the involvement of mPGES-1 in carcinogenesis has not yet been fully understood. In the present study, we used LLC (Lewis lung carcinoma) cells with mPGES-1 knockdown or overexpression, as well as mPGES-1-deficient mice to examine the roles of cancer cell- and host-associated mPGES-1 in the processes of tumorigenesis *in vitro* and *in vivo*. We found that siRNA (small interfering RNA) silencing of mPGES-1 in LLC cells decreased PGE_2 synthesis markedly, accompanied by reduced cell proliferation, attenuated Matrigel™ invasiveness and increased extracellular matrix adhesion. Conversely, mPGES-1-overexpressing LLC cells showed increased proliferating and invasive capacities. When implanted subcutaneously into wild-type mice, mPGES-1-silenced cells formed smaller xenograft tumours than did control cells. Furthermore, LLC tumours grafted subcutaneously into mPGES-1-knockout mice grew more slowly than did those grafted into littermate wild-type mice, with concomitant decreases in the density of microvascular networks, the expression of pro-angiogenic vascular endothelial growth factor, and the activity of matrix metalloproteinase-2. Lung metastasis of intravenously injected LLC cells was also significantly less obvious in mPGES-1-null mice than in wild-type mice. Thus our present approaches provide unequivocal evidence for critical roles of the mPGES-1-dependent PGE_2 biosynthetic pathway in both cancer cells and host microenvironments in tumour growth and metastasis.

Key words: knockout mouse, metastasis, microsomal prostaglandin E synthase-1, prostaglandin E_2, tumorigenesis.

INTRODUCTION

Numerous studies on rodent cancer models and human cancers have shown that NSAIDs (non-steroidal anti-inflammatory drugs) have antineoplastic properties [1]. A well-known effect of the NSAIDs is their ability to inhibit the enzyme COX (cyclo-oxygenase) and thereby to suppress PG (prostaglandin) synthesis. PGE_2, the most common PG, is involved in tumour progression by inducing angiogenesis, invasion and metastasis in several solid tumours [2]. Biosynthesis of PGE_2 from arachidonic acid, which is spatiotemporally supplied from membrane phospholipids by the action of phospholipase A_2, is catalysed sequentially by COX and PGES (PGE synthase) [3]. COX catalyses the insertion of molecular oxygen into arachidonic acid to form the unstable intermediate PGG_2, which is rapidly converted into PGH_2 by the peroxidase activity of the same enzyme. Of the two COX isoforms, COX-1 is expressed constitutively in most tissues and is generally responsible for the production of PGs that control normal physiological functions, whereas COX-2 is inducible in response to mitogens, cytokines and cellular transformation. High levels of constitutive expression of COX-2 and its product PGE_2 have been detected in various cancer cells and tissues. Moreover, pharmacological, cell biological and gene targeting studies investigating COX-2 and EPs (PGE receptors) have demonstrated that PGE_2 produced through the COX-2-dependent pathway contributes to the progression of several types of cancer [4,5].

PGES catalyses the conversion of PGH_2, produced by COX-1 or COX-2, into PGE_2. Thus far, three PGES enzymes, mPGES (microsomal PGES)-1, mPGES-2 and cPGES (cytosolic PGES), have been identified [6–9]. Among these PGES isozymes, mPGES-1 is induced by pro-inflammatory stimuli and down-regulated by anti-inflammatory glucocorticoids, as in the case of COX-2, and is functionally coupled with COX-2 in marked preference to COX-1 [7,10,11]. Induction of mPGES-1 expression and its function have been observed in various diseases and systems in which COX-2-driven PGE_2 has been implicated, such as rheumatoid arthritis, febrile response, reproduction, bone metabolism, cardiovascular function, stroke and Alzheimer's disease [12,13]. Furthermore, it has previously been reported

Abbreviations used: COX, cyclo-oxygenase; cPGES, cytosolic prostaglandin E synthase; DMEM, Dulbecco's modified Eagle's medium; dmPGE_2, 16,16-dimethyl prostaglandin E_2; ECM, extracellular matrix; EP, prostaglandin E receptor; FCS, fetal calf serum; GAPDH, glyceraldehyde-3-phosphate dehydrogenase; HEK, human embryonic kidney; KD, knockdown; KO, knockout; LLC, Lewis lung carcinoma; MMP, matrix metalloproteinase; mPGES, microsomal prostaglandin E synthase; NSAID, non-steroidal anti-inflammatory drug; PG, prostaglandin; PGES, PGE synthase; RT, reverse transcriptase; siRNA, small interfering RNA; TBS, Tris-buffered saline; TBS-Tween, TBS containing 0.05% Tween 20; VEGF, vascular endothelial growth factor; WT, wild-type.

[1] To whom correspondence should be addressed (email haras@pharm.showa-u.ac.jp).

[2] Professor Kudo died on April 27, 2008. We greatly miss him as a scientist and a friend. We offer sincere thanks to all the friends, colleagues and former collaborators of Professor Kudo who showed him kindness during his lifetime.

that mPGES-1 is constitutively expressed in several cancers, most of which also express COX-2 constitutively [14,15]. We have reported that the forcible transfection of mPGES-1 in combination with COX-2, but not with COX-1, into HEK (human embryonic kidney)-293 cells led to cellular transformation with a concomitant and robust increase in PGE_2 [14]. Transgenic mice overexpressing both COX-2 and mPGES-1 developed metaplasia, hyperplasia and tumorous growth in the glandular stomach with heavy macrophage infiltration [16,17]. It has also been suggested that the PGE_2 produced through the COX-2-dependent pathway may regulate cancer–host communications that influence tumour progression. Studies using mice null for COX-2 or EPs have revealed that stromal cells around cancer cells express COX-2 and synthesize PGE_2, which, in tumour niches, may act on stromal cells in an autocrine fashion to induce the production of pro-angiogenic factors and consequent angiogenesis, as well as on cancer cells in a paracrine fashion to promote their growth, survival, adhesion and motility [5,18–20]. Although several studies, including our own, have found, by immunohistochemistry, that mPGES-1 is expressed in both stromal cells and cancer cells in tumour tissues [14,21], the contribution of mPGES-1 expressed in either cell population to tumour progression has not yet been fully elucidated.

Although the inhibition of COX-2-mediated PGE_2 formation represents a promising chemopreventive strategy for reducing the risk of cancer, the cardiovascular side effects associated with COX-2 inhibitors, which most likely result from the blunting of anti-thrombotic prostacyclin (PGI_2), have previously been found to limit their use [22,23]. From this viewpoint, selective blockage of the biosynthesis of PGE_2 without affecting other prostanoids appears to be feasible for cancer chemoprevention with the potential for improved tolerability over NSAIDs. To better evaluate the efficacy of mPGES-1 inhibition in relieving symptoms of cancer, the present study used lung carcinoma cells with mPGES-1 KD (knockdown) or overexpression, as well as mice null for mPGES-1. Our results provide evidence that mPGES-1 in both cancer cells and hosts contributes to tumorigenesis *in vitro* and *in vivo*.

EXPERIMENTAL

Cells

LLC (Lewis lung carcinoma) cells, which were originally isolated from C57BL/6 mice, were cultured in DMEM (Dulbecco's modified Eagle's medium) containing 10% (v/v) FCS (fetal calf serum) under a humidified atmosphere containing 5% CO_2. To establish mPGES-1-KD and -overexpressing LLC cells, we transfected these cells with a pRNA-U6.1/Hygro siRNA (small interfering RNA) expression vector (GenScript) harboring an mPGES-1-directed siRNA target sequence [5′-GGCCTTTGCCAACCCCGAG-3′ (residues 126–144 in the open reading frame)] and a pcDNA3.1 expression vector (Invitrogen) containing mouse mPGES-1 cDNA respectively, using Lipofectamine™ 2000 (Invitrogen). After the transfection of these plasmids, LLC cells were cultured in medium containing 1 mg/ml G418 (Invitrogen) to establish stable clones. As a control, LLC cells transfected with an empty vector (pRNA-U6.1/Hygro or pcDNA3.1) were used (referred to as mock cells hereafter).

Animals

C57BL/6 and BALB/c mice were obtained from the Saitama Animal Center. mPGES-1-KO (knockout) mice were established as described previously [12,13], and backcrossed at least three generations with C57BL/6 mice or ten generations with BALB/c mice. Female mPGES-1-KO mice and littermate WT (wild-type) mice (7-weeks-old) were used in each experiment. The mice were housed in microisolator cages in a pathogen-free barrier facility, and all procedures involving animals were performed in accordance with protocols approved by the Institutional Animal Care and Use Committee of Showa University, in accordance with the Standards Relating to the Care and Management of Experimental Animals in Japan.

Cell growth assay

Cells were seeded at 6×10^4 cells/well in six-well plates or 1.5×10^5 cells/flask in T-25 culture flasks in culture medium in the presence or absence of 10 nM NS-398 (Cayman Chemicals), a COX-2 selective inhibitor, or 1 mM $dmPGE_2$ (16,16-dimethyl PGE_2) (Cayman Chemicals), a metabolically stable analogue of PGE_2. After culture for 72 h, the cells were collected by trypsinization and counted in a Bright-line haemocytometer in the presence of Trypan Blue.

Western blot analysis

Aliquots of samples (20 μg of protein equivalents) were subjected to SDS/PAGE using 10% (w/v) gels under reducing conditions. The separated proteins were electroblotted on to nitrocellulose membranes (Schleicher & Schuell) with a semi-dry blotter (Bio-Rad). After blocking with 3% (w/v) dried non-fat skimmed milk in TBS (Tris-buffered saline) (pH 7.4) containing 0.05% Tween 20 (TBS-Tween), the membranes were probed with the respective antibodies for 2 h {1:2000 dilution for antibodies against mPGES-1 [14], mPGES-2 (Cayman Chemicals), cPGES [11], COX-1 and -2 (Santa Cruz Biotechnology), EP1, 2, 3 and 4 (Cayman Chemicals), and VEGF (vascular endothelial growth factor; Sigma); and 1:2500 dilution for anti-mouse α-tubulin antibody (Zymed Laboratories) in TBS-Tween}. After washing with TBS-Tween, the membranes were incubated with horseradish peroxidase-conjugated anti-goat (for COX-1, COX-2 and VEGF), anti-rabbit (for mPGES-1, mPGES-2, cPGES and EP1–4) and anti-mouse (for α-tubulin) IgG antibodies (1:5000 dilution in TBS-Tween) for 1 h, and visualized with the ECL (enhanced chemiluminescence) Western blot system (PerkinElmer Life Sciences), as described previously [7,13,14]. Amounts of individual proteins relative to that of α-tubulin were estimated from their signal intensities on the Western blots using Lane and Spot Analyzer (ATTO).

Determination of PG levels

For the measurement of PGs in tissues, mouse tissues were washed twice with Hank's balanced salt solution containing 10 μM indomethacin (Sigma) before homogenization. The supernatants obtained from the tissue homogenates were adjusted to pH 3.0 with 1 M HCl and passed through a Sep-Pak C_{18} cartridge (Waters), and the retained PGs were eluted with 8 ml of methanol, as described previously [13]. A trace amount of [^{3}H]PGE_2 (Cayman Chemicals) was added to the samples before passage through the cartridges to calibrate the recovery of the PGs. The sample solvents were evaporated, and then the PGs were dissolved in an aliquot of buffer and assayed with commercial enzyme immunoassay kits for individual PGs (Cayman Chemicals). Likewise, aliquots of the supernatants of cultured cells were subjected to the enzyme immunoassay for PGs.

Adhesion assay

Cells were plated at 2×10^5 cells in 35-mm dishes, which were pre-treated with collagen, fibronectin or laminin (BD Biosciences). After incubation for 60 min at 37 °C, the cells were fixed with Carnoy solution and then stained with Giemsa solution for 60 min. Adherent cells were counted in three fields at ×40 magnification using a microscope and J image software.

Invasion assay

Cell invasiveness was evaluated using a BD BioCoat™ Matrigel™ Invasion Chamber (BD Biosciences) according to the manufacturer's instructions. In brief, cells (1.2×10^6 cells in 0.5 ml) suspended in DMEM containing 3 % (v/v) FCS and 1 % (v/v) sodium pyruvate (Invitrogen) were seeded on the top of the gel in each chamber. DMEM containing 10 % (v/v) FCS (0.75 ml) was added as a source of chemoattractants into the bottom wells of the plate. After 16 h of incubation, cells that had invaded on to the lower surface of the chamber were fixed with methanol for 5 min, and stained with Crystal Violet. Non-invasive cells on the upper surface were removed with a cotton bud, and the membrane was cut. The number of invading cells was quantified by counting them under a light microscope. Statistical significance was determined using the Student's t test.

Tumour implantation model

LLC cells (1×10^6) in 100 μl of PBS were injected subcutaneously into 8-week-old female mice. Tumour growth was assessed by the measurement of two bisecting diameters in each tumour using calipers. The size of the tumour was determined by direct measurement of the tumour dimensions. The volume was calculated according to the equation: $V = (L \times W^2) \times 0.5$, where V = volume, L = length and W = width [35]. On day 14 after tumour implantation, the mice were anaesthetized and killed by dislocation of the cervical spine, and the tumour tissues were dissected, weighed and then fixed in 10 % (v/v) formalin for histochemical analyses. The intratumoral blood vessels in the most intensive neovascularization areas were quantified by staining of the sections with haematoxylin and eosin followed by silver. For each tumour, five random images were captured at ×400 magnification. Only areas of viable tumour tissue were imaged; necrotic regions were excluded. The individual microvessels were counted. The structure of individual microvessels was clearly differentiated from tumour cells on silver staining. The final vascular density score for the tumour represents an average of all scored fields.

Lung metastasis model

LLC cells (1×10^6) in 100 μl of PBS were intravenously injected into the lateral tail veins of 8-week-old female mice. Then, 14 days later, the mice were anaesthetized and killed, and the lungs were removed and weighed. Finally, the lungs were placed in Bouin's solution for 24 h and then photographed.

Determination of haemoglobin levels in tumour tissues

The dissected tumour tissues were washed, cut into small pieces with scissors, and homogenized with a Polytron homogenizer in a SET buffer [250 mM sucrose, 0.5 mM EDTA and 20 mM Tris/HCl (pH 7.4)] containing 10 μM indomethacin, 1 mM PMSF and 0.5 % Triton X-100. The tissue homogenates obtained were centrifuged at 600 g for 5 min, and an aliquot (200 μl) of the supernatant was centrifuged again at 14 000 g for 30 min at 4 °C. Concentrations of haemoglobin in the supernatant were then determined spectrophotometrically by measuring the absorbance at 540 nm using a haemoglobin assay kit (Wako).

RT (reverse transcriptase)–PCR

Total RNA was isolated from cells and tissues using TRIzol® (Invitrogen). Synthesis of cDNA was performed with 2 μg of the total RNA and avian myeloblastosis virus RT according to the manufacturer's instructions supplied with the RNA PCR kit version 2.1 (Takara Biomedicals). Subsequent amplifications of the partial cDNA fragments were performed using 0.5 μl of the reverse-transcribed mixture as a template with a set of specific oligonucleotide primers (Sigma) as follows: (i) mouse VEGF, sense 5′-GATGAAGCCCTGGAGTGC-3′ and antisense 5′-TCCCAGAAACAACCCTAA-3′; and (ii) mouse GAPDH (glyceraldehyde-3-phosphate dehydrogenase), sense 5′-TCGTGGATCTGACGTGCCGCCTG-3′ and antisense 5′-CACCACCCTBTTGCTGTAGCCGTAT-3′. The PCR mixtures were subjected to 30 cycles of amplification by denaturation (30 s at 94 °C), annealing (30 s at 57 °C) and elongation (30 s at 72 °C). The PCR products were analysed by 1 % (w/v) agarose gel electrophoresis with ethidium bromide.

Real-time RT–PCR

Single-stranded cDNA was generated using 1 μg of total RNA as a template and avian myeloblastosis virus RT, using a high capacity reverse transcriptase kit (Applied Biosystems). Real-time PCR was carried out using the SYBR Green PCR Master Mix (Applied Biosystems) and StepOne (Applied Biosystems) according to the manufacturer's instructions. The PCR primer sets used were: (i) mouse EP2, sense 5′-GCTGTGCTCGCCTGCAA-3′ and antisense 5′-CGACGGTGCATGCGAAT-3′; (ii) mouse EP4, sense 5′-CATCATCTGTGCCATGAGCAT-3′ and antisense 5′-GCTGTAGAAGTAGGCGTGGTTGA-3′; (iii) mouse VEGF, sense 5′-TACCTCCACCATGCCAAGTG-3′ and antisense 5′-TGGGACTTCTGCTCTCCTTCTG-3′; (iv) mouse MMP (matrix metalloproteinase)-2, sense 5′-GGACCCCGGTTTCCCTAA-3′ and antisense 5′-CAGGTTATCAGGGATGGCATTC-3′; (v) mouse MMP-9, sense 5′-AGTGGGACCATCATAACATCACAT-3′ and antisense 5′-TCTCGCGGCAAGTCTTCAG-3′; (vi) mouse α5 integrin, sense 5′-ATGGCTCAGACATCCACTCC-3′ and antisense 5′-GGTCATCTAGCCCATCTCCA-3′; and (vii) mouse β1 integrin, sense 5′-GGTGTCGTGTTTGTGAATGC-3′ and antisense 5′-TGACGCTAGACATGGACCAG-3′. The expression levels of EP2, EP4, MMP-2, MMP-9 and integrins were normalized with those of mouse GAPDH with a primer set of 5′-ATGTGTCCGTCGTGGATCTGA-3′ and 5′-ATGCCTGCTTCACCACCTTCT-3′. Results represent an average of several independent experiments.

Gelatin zymography

Lysates of cells and tissues (27 μg of protein equivalents) were subjected to SDS/PAGE (10 % gels), with 1 mg/ml gelatin substrate being incorporated into the gels. Following electrophoresis, the gels were soaked in 2.5 % Triton X-100 to remove SDS, rinsed with 10 mM Tris/HCl (pH 8.0), and transferred to a bath containing 50 mM Tris/HCl(pH 8.0), 5 mM $CaCl_2$ and 1 μM $ZnCl_2$ at 37 °C for 18 h. The gels were then stained with 0.1 % Coomassie Blue in 45 % methanol and 10 % acetic acid.

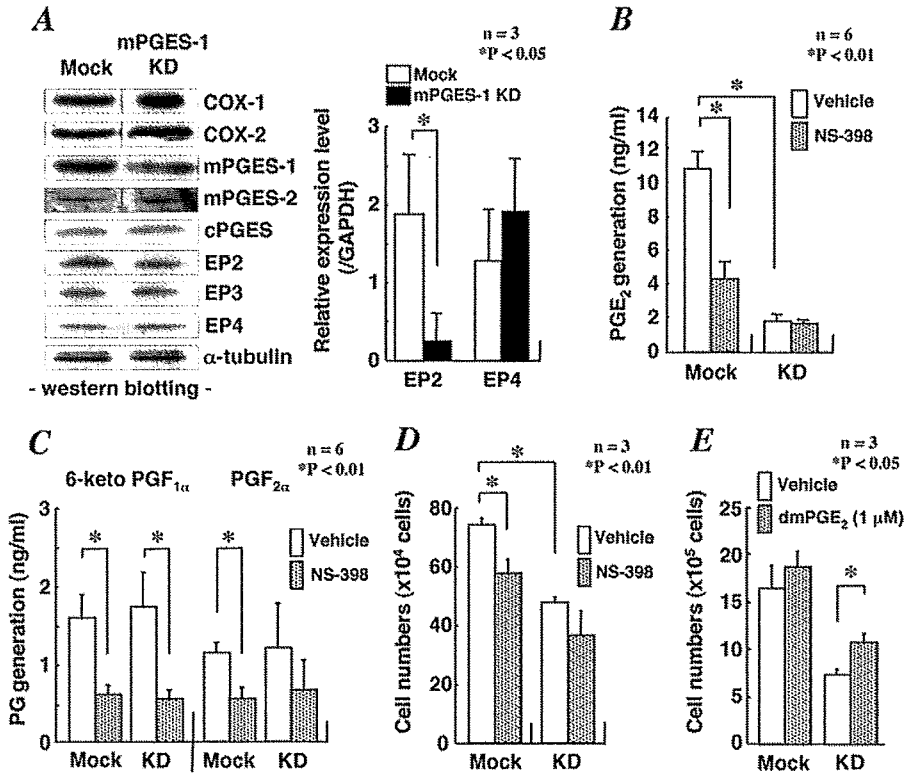

Figure 1 PGE_2 production and cell proliferation in mPGES-1-silenced LLC cells *in vitro*

(**A**) Expression of PGE_2 biosynthetic enzymes and PGE receptors in mPGES-1-KD and control (mock) cells was assessed by immunoblotting (left-hand panel). Equal amounts of cell lysates (20 μg of protein equivalents) were separated by SDS/PAGE and analysed by Western blotting at the same time with the corresponding antibodies to allow for a direct comparison. Representative results of at least three experiments are shown. Expression levels of EP2 and EP4 mRNAs in KD and mock cells were evaluated by quantitative RT–PCR, with GAPDH mRNA used for normalization (right-hand panel). (**B–D**) Effects of mPGES-1 silencing and 10 nM NS-398, a COX-2 selective inhibitor, on production of PGE_2 (**B**), 6-keto $PGF_{1\alpha}$ and $PGF_{2\alpha}$ (**C**), and on cell proliferation (**D**). mPGES-1-KD and mock cells were seeded at 6×10^4 cells/well in six-well culture dishes in the presence or absence of 10 nM NS-398. After culture for 3 days, the cells were collected and counted in a Bright-line haemocytometer in the presence of Trypan Blue, and the supernatants were taken for enzyme immunoassay of several PGs. (**E**) Effect of $dmPGE_2$ on cell proliferation. mPGES-1-KD and mock cells were seeded in T-25 culture flasks at 1.5×10^5 cells/flask in culture medium in the presence or absence of 1 μM $dmPGE_2$. After culture for 3 days, the cells were collected and counted. Values are the means $\pm$ S.E.M. Similar results were obtained in three independent cell lines of mPGES-1-KD and control cells.

RESULTS

Reduced tumorigenic potential of mPGES-1-silenced LLC cells *in vitro*

We established mPGES-1-KD LLC cells by means of an siRNA-silencing strategy, as described in the Experimental section. The expression levels of mPGES-1 and other enzymes involved in PGE_2 synthesis in mPGES-1-KD and mock cells were examined by Western blot analysis (Figure 1A). The expression level of mPGES-1 was reduced by ~80% in mPGES-1-KD cells relative to mock cells, whereas those of COX-1 and -2 and other PGE synthases (cPGES and mPGES-2) in both cell lines were approximately the same (Figure 1A, left-hand panel). Furthermore, we found that, among the four EP receptor subtypes that can bind to PGE_2 [24], LLC cells expressed detectable levels of EP2, EP3 and EP4 proteins, among which the level of EP2 protein was reduced in mPGES-1-KD cells relative to mock cells, whereas the levels of EP3 and EP4 were unaffected by mPGES-1 silencing (Figure 1A, left-hand panel). The reduction in EP2, but not EP4, expression in the KD cells was verified by quantitative RT–PCR (Figure 1A, right-hand panel) and quantifying individual immunoblots by a densitometer (Supplementary Figure S1 at http://www.BiochemJ.org/bj/425/bj4250361add.htm). The amounts of PGE_2 released into the medium during culture were decreased in mPGES-1-KD cells relative to mock cells (Figure 1B), whereas those of 6-keto $PGF_{1\alpha}$ (a non-enzymatic hydrolytic product of PGI_2) and $PGF_{2\alpha}$ were comparable between mPGES-1-KD cells and mock cells (Figure 1C).

Concurrently, mPGES-1-KD cells grew more slowly than did mock cells (Figure 1D). NS-398, a COX-2-selective inhibitor, suppressed PGE_2 generation and cell proliferation in mock cells by ~60% and ~25% respectively, whereas no further decreases in PGE_2 production and cell growth were found in mPGES-1-KD cells (Figures 1B and 1D). Production of 6-keto $PGF_{1\alpha}$ and $PGF_{2\alpha}$ was equally sensitive to NS-398 in both cell lines (Figure 1C). Furthermore, cell growth of mPGES-1-KD cells was partially (even if not completely, probably because EP2 expression was reduced in the KD cells; see above) restored by addition of an optimal concentration (1 μM) of $dmPGE_2$, a synthetic analogue of PGE_2 (Figure 1E). These results suggest that the PGE_2 produced through the COX-2/mPGES-1 pathway is partially required for the proliferation of LLC cells.

In the process of tumour metastasis, cancer cells from the primary tumour must invade the ECM (extracellular matrix). There are many reports demonstrating that malignant tumour cells often possess high invasive activity [25]. Thus we next assessed the effect of mPGES-1 silencing on the invasive activity of LLC cells using Matrigel™ invasion chambers. As shown in Figure 2(A), the number of mPGES-1-KD cells migrating across the Matrigel™-coated filter was markedly fewer than that of mock cells. Since it is known that the PGE_2 signalling activates the invasive potential of cancer cells by increasing the expressions

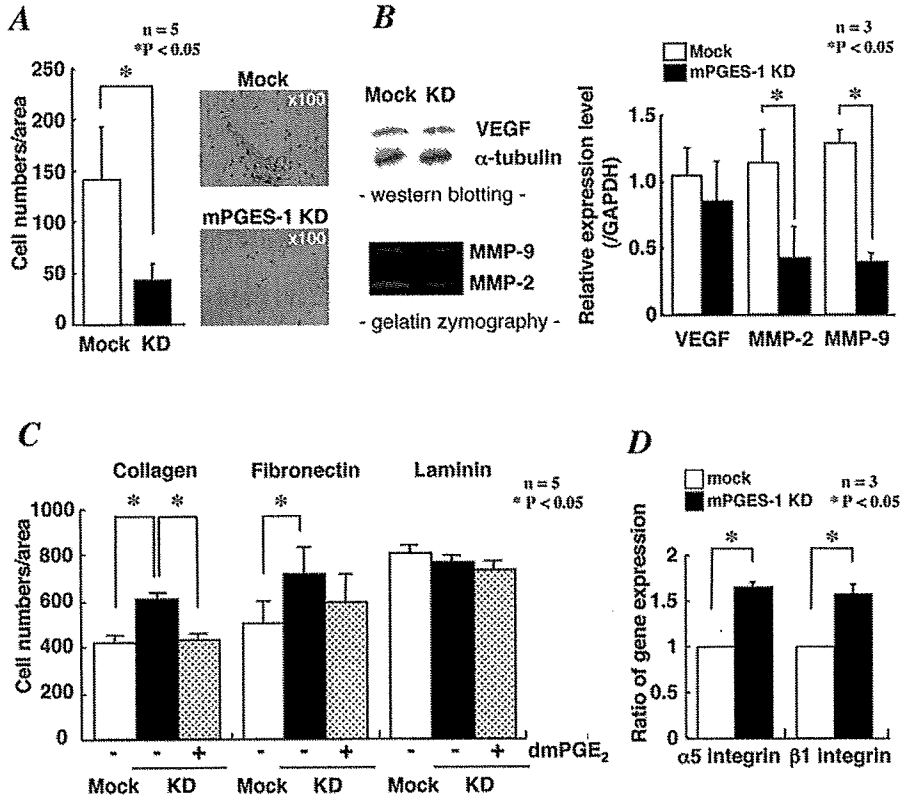

Figure 2 siRNA silencing of mPGES-1 in LLC cells reduces their malignant potential *in vitro*

(**A**) mPGES-1-KD and mock cells [1.2×10^6 cells in DMEM containing 3% (v/v) FCS] were seeded on to the upper wells of BD BioCoat™ Matrigel™ Invasion Chambers. DMEM containing 10% (v/v) FCS was added as a source of chemoattractants into the bottom wells of the plates. After 16 h of incubation, cells that had invaded on to the lower surface of the chambers were fixed, stained with Crystal Violet and counted (left-hand panel). Values are the means ± S.E.M. of five independent experiments. Representative photographs of mPGES-1-KD and mock cells that invaded across the Matrigel™-coated inserts are shown (right-hand panel). (**B**) The expression of VEGF protein in mPGES-1-KD and mock cells was assessed by immunoblotting (upper panel). The cell lysates (20 μg of protein equivalents) were separated by SDS/PAGE and then subjected to Western blot analysis using anti-VEGF and anti-α-tubulin antibodies. The activities of MMP-2 and -9 in mPGES-1-KD and mock cells were assessed by gelatin zymography (lower panel). Lysates of cells (27 μg of protein equivalents) were subjected to SDS/PAGE containing 1 mg/ml gelatin. Following electrophoresis, the gels were incubated in a bath containing 1 μM $ZnCl_2$ at 37°C for 18 h. The gels were then stained with 0.1% Coomassie Blue. The expression levels of mRNAs for VEGF, MMP-2 and MMP-9 were evaluated by quantitative RT–PCR, with GAPDH mRNA used for normalization (means ± S.D.; $n = 3$) (right-hand panel). (**C**) Adhesion of mPGES-1-KD and mock cells to ECM proteins. mPGES-1-KD or mock cells (2×10^5 cells) were seeded on to 35-mm dishes coated with collagen, fibronectin or laminin in culture medium in the presence or absence of 1 μM $dmPGE_2$. After allowing cells to attach for 60 min at 37°C, non-adherent cells were removed by washing. Adherent cells were fixed and stained with Giemsa solution and counted in three fields at ×40 magnification using a microscope and J image software. Values are the means ± S.E.M. of five independent experiments. (**D**) Expression of α5 and β1 integrins in mPGES-1-KD and mock cells. Total RNA was isolated from mPGES-1-KD and mock cells and subjected to quantitative RT–PCR using specific primers of α5 (left-hand panel) and β1 (right-hand panel) integrins and those of GAPDH as a reference. The results of quantitative RT–PCR were normalized with their expression in mock cells being regarded as 1 (means ± S.D., $n = 3$). Similar results were obtained in two independent cell lines of mPGES-1-KD and control cells.

of VEGF, a pro-angiogenic factor, and MMPs, which hydrolyse type IV collagen localized in the basement membrane [25], we next examined the effects of mPGES-1 silencing on the expression of VEGF and the activities of MMP-2 and -9 by Western blot analysis, gelatin zymography and quantitative RT–PCR. As shown in Figure 2(B), the activities of MMP-2 and -9 in the conditioned medium from mPGES-1-KD cells were lower than those in the medium from mock cells. Consistently, expression levels of both MMP-2 and -9 mRNAs were significantly reduced in the KD cells relative to control cells. In contrast, the levels of VEGF protein and mRNA were unaffected by mPGES-1 silencing (Figure 2B). These results suggest that the silencing of mPGES-1 diminishes *in vitro* migration of LLC cells by reducing the PGE_2-induced expression of MMP-2 and -9.

The ability of cancer cells to adhere to the ECM influences their motility and invasion in tumour tissues *in vivo*, and metastatic tumour cells show decreased ECM-adherent activity *in vitro* [25,26]. Therefore we next studied the attachment of mPGES-1-KD or mock cells to culture dishes pre-coated with distinct ECM components. The results showed that the numbers of mPGES-1-KD cells adhering to collagen and fibronectin, but not to laminin, were significantly increased as compared with those of mock cells (Figure 2C). Moreover, the increased adhesion of mPGES-1-KD cells to collagen was reversed by $dmPGE_2$ to the level of mock cells, and adhesion of the cells to fibronection also showed a similar trend (Figure 2C). Consistent with the increased binding of mPGES-1-KD cells to collagen and fibronectin, the expressions of their receptor components, α5 and β1 integrins, were elevated in the KD cells relative to control cells (Figure 2D). Thus we conclude that mPGES-1 supplies a majority of the PGE_2 that enhances the malignant potential (in terms of ECM invasion and adherence) of cancer cells.

Increased tumorigenic potential of mPGES-1-overexpressing LLC cells *in vitro*

We next established LLC cells that stably overexpressed mPGES-1 and examined whether these cells (as opposed to

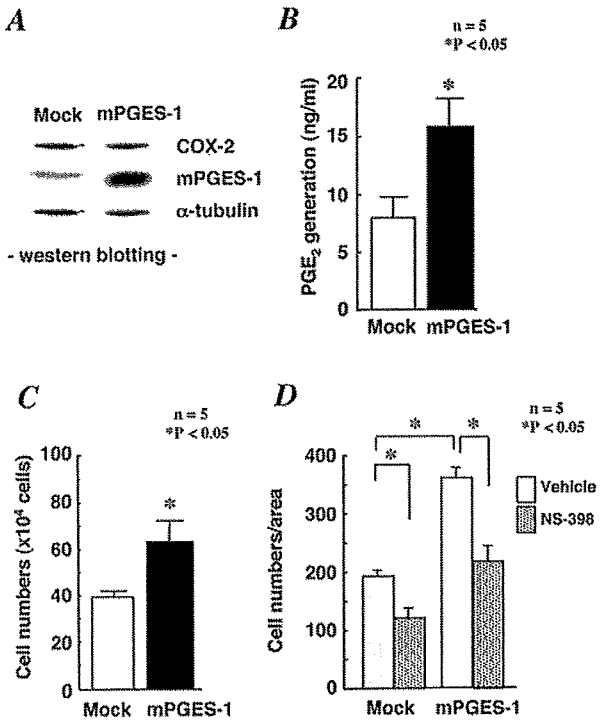

Figure 3 Increased PGE_2 generation, proliferation and invasion of mPGES-1-overexpressing LLC cells

(**A**) Expression of COX-2 and mPGES-1 in mPGES-1-overexpressing and mock cells was assessed by Western blot analysis. Representative results of at least three experiments are shown. (**B** and **C**) Effects of mPGES-1 overexpression on PGE_2 generation (**B**) and cell growth (**C**). mPGES-1-overexpressing and mock cells were seeded at 6×10^4 cells/well in six-well culture dishes. After culture for 2 days, the cells were collected and counted, and the supernatants were taken for a PGE_2 enzyme immunoassay. Values are the means ± S.E.M. of five independent experiments. (**D**) mPGES-1-overexpressing and mock cells (1.2×10^6 cells in the presence or absence of 10 nM NS-398) that had invaded through BD BioCoat™ Matrigel™ Invasion Chamber inserts over 16 h were counted. Values are the means ± S.E.M. of five independent experiments. Similar results were obtained in two independent cell lines of mPGES-1-overexpressing and mock cells.

mPGES-1-KD cells) would show increased proliferation and invasion. mPGES-1-transfected LLC cells expressed more mPGES-1 protein than did mock cells, whereas the expression of COX-2 protein was unaltered (Figure 3A). PGE_2 release into the medium during culture was increased by ~2-fold in mPGES-1-overexpressing cells relative to mock cells (Figure 3B). As shown in Figure 3(C), the growth rate of mPGES-1-overexpressing cells was significantly faster than that of mock cells. Moreover, the Matrigel™ invasion chamber assay revealed that the invasive activity of mPGES-1-overexpressing cells was notably higher than that of mock cells (Figure 3D). Additionally, treatment of both mock and mPGES-1-overexpressing LLC cells with NS-398 reduced the invasion by ~40% (Figure 3D). These results confirm that the increased production of PGE_2 through the COX-2/mPGES-1 pathway in cancer cells facilitates their proliferation and invasion.

Silencing of mPGES-1 in cancer cells reduces tumorigenesis *in vivo*

To assess the contribution of mPGES-1 in cancer cells to tumour development *in vivo*, we grafted mPGES-1-KD and mock LLC cells subcutaneously into BALB/c mice, and the development of the solid tumour around the injection sites was evaluated on day 14 after implantation. Remarkably, both the volume and mass of xenografts derived from mPGES-1-KD cells were significantly smaller than those derived from mock cells (Figures 4A and 4B). The levels of prostanoids (PGE_2, $PGF_{2\alpha}$ and 6-keto-$PGF_{1\alpha}$) in the homogenates of xenografts did not differ significantly between the genotypes, even though PGE_2 tended to decrease in the xenografts from mPGES-1-KD cells compared with those from mock cells (Figure 4C). The expression of VEGF, as assessed by RT–PCR and quantitative RT–PCR, was reduced in mPGES-1-KD xenografts as compared with control xenografts (Figure 4D). Considering that VEGF expression was unaltered by silencing of mPGES-1 in LLC cells *in vitro* (Figure 2B), the reduction of VEGF expression in mPGES-KD xenografts *in vivo* may reflect the action of mPGES-1-derived PGE_2 from cancer cells on proximal stromal cells in tumour microenvironments.

Reduced tumour growth and angiogenesis in mPGES-1-KO mice

The observations described above indicate that cancer cell-associated COX-2 and mPGES-1 co-operatively produce PGE_2, which accelerate multiple steps of malignant progression, including cell proliferation, invasion and ECM adhesion. In terms of the pathological circumstances, it has been reported that COX-2 and mPGES-1 are expressed not only in tumour cells, but also in the stromal cells (mainly in infiltrating macrophages) surrounding them [14,21]. To investigate the contribution of host-associated mPGES-1 to tumour growth, we next grafted parental LLC cells subcutaneously into either mPGES-1-KO or WT mice, and evaluated the development of solid tumour around the injection sites. Although the absence of mPGES-1 in the host mice influenced neither the engraftment rate nor the growth of tumours during the first 5 days after implantation, tumours grafted into the mPGES-1-KO mice were significantly smaller in size than those grafted into the WT mice after day 6 and beyond (Figure 5A). On day 14 after implantation, the tumour mass in mPGES-1-KO mice was reduced to half of that in WT mice (Figure 5B, left-hand panel). The levels of PGE_2 in homogenates of the dissected tumour tissues were nearly 50% less in mPGES-1-KO mice than in WT mice, whereas those of $PGF_{2\alpha}$ were unaffected by the host mPGES-1 deficiency (Figure 5B, right-hand panel).

Histological examination of the xenografts revealed that the vascularization of tumour tissues was markedly reduced by the lack of host mPGES-1 expression (Figure 5C, indicated by arrowheads). The vascular density was approx. 60% lower in tumours grafted in mPGES-1-KO mice than those grafted in WT mice (Figure 5D, left-hand panel). The haemoglobin contents in the tumour tissues, which appeared to be well correlated with tumour neovascularization upon histological examination [30], were also reduced in mPGES-1-KO mice in comparison with that in WT mice (Figure 5D, right-hand panel). The reduction of tumour angiogenesis in mPGES-1-KO mice caused a large area of central necrosis in the xenografts of mPGES-1-KO, but not WT, mice (Figure 5C, indicated by an asterisk). We further found that the expression levels of the VEGF protein and mRNA in tumour tissues were also markedly lower in mPGES-1-KO mice than in WT mice (Figure 5E, left-hand panel). The decrease in VEGF protein in the xenografts of mPGES-1-KO mice was confirmed by quantification of the relative abundance of VEGF to α-tubulin using a densitometer (Figure 5E, right-hand panel). These results suggest that host mPGES-1-derived PGE_2 plays a pivotal role in tumour-associated VEGF production and accompanying angiogenesis. Again, considering that VEGF expression was

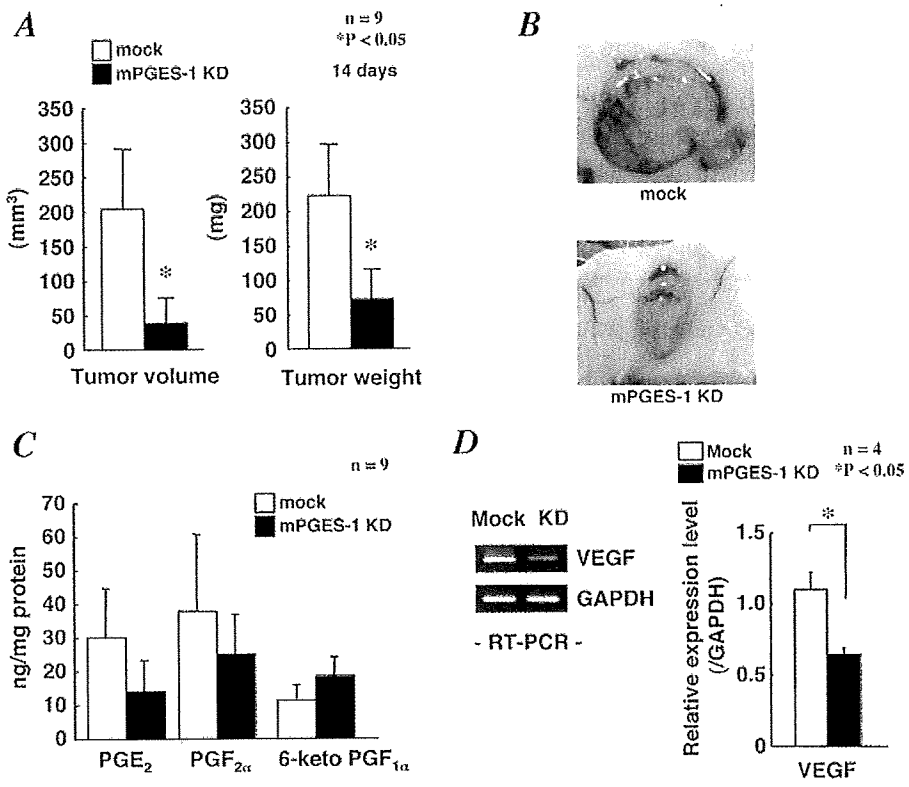

Figure 4 siRNA silencing of mPGES-1 in cancer cells reduces tumorigenesis *in vivo*

(**A–C**) mPGES-1-KD or mock cells (10^6 cells) were injected into the subcutaneous tissue of female BALB/c mice. On day 14 after implantation, tumour volume was scored according to the formula $V = (L \times W^2) \times 0.5$ (**A**, left-hand panel). The tumour tissues were photographed at × 100 magnification (**B**), dissected and weighed (**A**, right-hand panel). Values are means ± S.E.M. ($n = 9$). (**C**) Amounts of PGE_2, $PGF_{2\alpha}$ and 6-keto $PGF_{1\alpha}$ in homogenates of the tumour tissues were quantified by enzyme immunoassay (means ± S.E.M., $n = 9$). (**D**) Expression of VEGF in tumour xenografts of mPGES-1-KD and mock cells was assessed by RT–PCR followed by electrophoresis (left-hand panel) and quantitative RT–PCR (right-hand panel), with the expression of GAPDH as a reference (means ± S.D., $n = 4$).

unaltered in mPGES-1-KD cells *in vitro* (Figure 2B), the reduced expression of this angiogenic factor in tumour tissue in mPGES-1-KO mice may reflect the impact of mPGES-1-derived PGE_2 on tumour microenvironments rather than on tumour cells *in vivo*.

We further examined the role of host-associated mPGES-1 in tumour metastasis by intravenous injection of parental LLC cells into mPGES-1-KO and WT mice. After 14 days, macroscopic metastases, as assessed by Bouin's staining, were found in the lungs of both genotypes, but the number and size of metastatic foci (Figure 6A) and the mass (Figure 6B, left-hand panel) of the lungs were significantly reduced in mPGES-1-KO mice compared with WT mice. Levels of PGE_2 were reduced by nearly 50 % in homogenates of the lungs from mPGES-1-KO mice relative to WT mice (Figure 6B, right-hand panel). Moreover, as assessed by RT–PCR and quantitative RT–PCR, VEGF expression in the metastasized lungs was significantly lower in mPGES-1-KO mice than in WT mice (Figures 6C and 6E). Gelatin zymography revealed that the activity of MMP-2 in the metastasized lung tissues was mitigated in mPGES-1-KO mice in comparison with that in WT mice (Figure 6D), and the levels of both MMP-2 and -9 mRNAs were significantly lower in the lung of mPGES-1-KD mice than in that of WT mice (Figure 6E). Collectively, these results indicate that host mPGES-1-driven PGE_2 plays a role in promoting tumour development and metastasis, which was associated with increased VEGF expression and MMP-2 and -9 activation.

DISCUSSION

Although the concept that the PGE_2 produced through the COX-2-dependent pathway participates in the pathogenesis of several types of cancer has been well established in the past decade based on a series of genetic studies employing mice ablated for the biosynthetic enzymes (COX-2) and receptors (EPs) or pharmacological studies employing inhibitors or agonists/antagonists fairly specific for them, the contribution of a step between COX-2 and EPs, namely PGES enzymes that convert COX-2-produced PGH_2 into PGE_2, to cancer development has remained incompletely understood. In this context, we have previously shown that co-transfection of mPGES-1 in combination with COX-2 into HEK-293 cells leads to a malignant phenotype [14]. In our continuing efforts to gain further insights into the role of mPGES-1 in tumorigenesis, we used two approaches in the present study. First, we performed siRNA-mediated silencing and overexpression of mPGES-1, which enabled us to address the complementary effects of endogenous compared with overexpressed mPGES-1 in cancer cells on tumorigenic potentials (growth, invasion and ECM binding *in vitro* and tumour xenograft propagation *in vivo*). Secondly, implantation of carcinoma cells into mPGES-1-KO mice and WT mice allowed us to evaluate the contribution of mPGES-1 expressed in tissue microenvironments to the development and metastasis of tumours in proximal and distant tissues. Our results clearly indicate that mPGES-1 expressed in both cancer cells and